# UV Spectropolarimetry with *Polstar*: Massive Star Binary Colliding Winds

Nicole St-Louis\*,<sup>1</sup>, Ken Gayley<sup>2</sup>, D. John Hillier<sup>3</sup>, Richard Ignace<sup>4</sup>, C. E. Jones<sup>5</sup>, Alexandre David-Uraz<sup>6,7</sup>, Noel D. Richardson<sup>8</sup>, Jorick S. Vink<sup>9</sup>, Geraldine J. Peters<sup>10</sup>, Jennifer L. Hoffman<sup>11</sup>, Yaël Nazé<sup>12</sup>, Heloise Stevance<sup>13</sup>, Tomer Shenar<sup>14</sup>, Andrew G. Fullard<sup>15</sup>, Jamie R. Lomax<sup>16</sup> and Paul A. Scowen<sup>17</sup>

\*Corresponding author(s). E-mail(s): nicole.st-louis@umontreal.ca;

#### Abstract

The winds of massive stars are important for their direct impact on the interstellar medium, and for their influence on the final state of a star prior to it exploding as a supernova. However, the dynamics of these winds is understood primarily via their illumination from a single central source. The Doppler shift seen in resonance lines is a useful tool for inferring these dynamics, but the mapping from that Doppler shift to the radial distance from the source is ambiguous. Binary systems can reduce this ambiguity by providing a second light source at a known radius in the wind, seen from orbitally modulated directions. From the nature of the collision between the winds, a massive companion also provides unique additional information about wind momentum fluxes. Since massive stars are strong ultraviolet (UV) sources, and UV resonance line opacity in the wind is strong, UV instruments with a high resolution spectroscopic capability are essential for extracting this dynamical information. Polarimetric capability also helps to further resolve ambiguities in aspects of the wind geometry that are not axisymmetric about the line of sight, because of its unique access to scattering direction information. We review how the proposed MIDEX-scale mission Polstar can use UV spectropolarimetric observations to critically constrain the physics of colliding winds, and hence radiatively-driven winds in general. We propose a sample of 20 binary targets, capitalizing on this unique combination of illumination by companion starlight, and collision with a companion wind, to probe wind attributes over a range in wind strengths. Of particular interest is the hypothesis that the radial distribution of the wind acceleration is altered significantly, when the radiative transfer within the winds becomes optically thick to resonance scattering in multiple overlapping UV lines.

**Keywords:** Ultraviolet astronomy (1736); Ultraviolet telescopes (1743); Space telescopes (1547); Massive stars (732), Binary stars (154), Stellar winds (1636); Spectropolarimetry (1973); Polarimeters (1277), Instruments: Polstar; UV spectropolarimetry; NASA: MIDEX

### 1 Introduction

Despite comprising the rarest stellar mass group, massive stars ( $> 8 M_{\odot}$ ) are amongst the most important originators of elements in the Universe because they synthesize and distribute heavy elements, especially oxygen through aluminum,

when they explode as supernova. They also form and evolve much faster than lower-mass stars, thereby influencing the formation and composition of all other stars and their planets. The drastically stronger stellar wind of a massive star, when compared to the solar wind, also enriches

the interstellar medium, and can lead to significant changes in the star's mass over its lifetime. This affects its evolutionary path in the H-R diagram, its type of supernova, whether it becomes a gamma-ray burster, and the compact remnant it produces, along with any gravitational wave signature it might create if it is a close binary.

Indeed, most massive stars spend a large fraction of their lives in binary systems with other massive stars, and more than half are thought to engage in mass exchange with a close companion (Sana et al, 2012). Tracking these evolutionary effects are the topic of two other *Polstar* proposal objectives (Jones et al, 2022; Peters et al, 2022); this paper relates to the objective that entails using the proximity of the two massive stars as a unique probe of the nature of their wind dynamics.

### 1.1 Wind Acceleration and Stratification

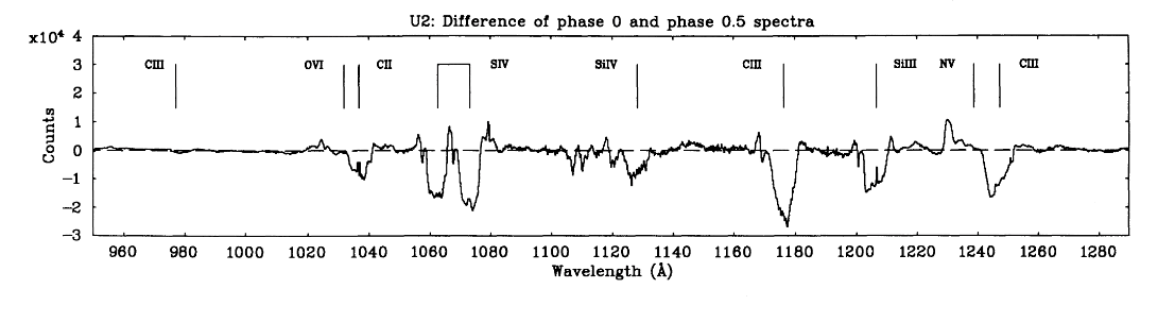
Over the past few decades our understanding of radiatively-driven hot, massive-star winds has greatly improved. But despite this observational and theoretical progress, fundamental details of radiatively driven winds, such as the velocity structure, still elude us. The so-called  $\beta - law$ , although extremely convenient to describe the general density structure of massive-star winds, does not arise from a solid physical description of the winds; it rests on an unlikely simplification that the wind opacity does not undergo significant change as the wind temperature and density drop with radius, and as the radiation field shifts from primarily diffusive to primarily radially streaming. Attempts to better describe the radial acceleration profile of hot-star winds have been made over the years, such as adjusting the value of the  $\beta$  exponent, or in the case of WR stars, adopting a typical value of that exponent in the inner wind, while using in the outer wind a higher value describing a second extended acceleration regime (Hillier and Miller, 1999; Gräfener and Hamann, 2005). More recently, Sander et al (2020) presented hydrodynamically consistent models of classical WR stars and find that a traditional  $\beta - law$  is inadequate for mass-loss rates above  $10^{-6} \text{ M}_{\odot} \text{ yr}^{-1}$  (see also Gräfener and Hamann, 2005). Instead, a plateau in the velocity law develops due to the decrease of the radiative acceleration between the two opacity bumps (hot and cool).

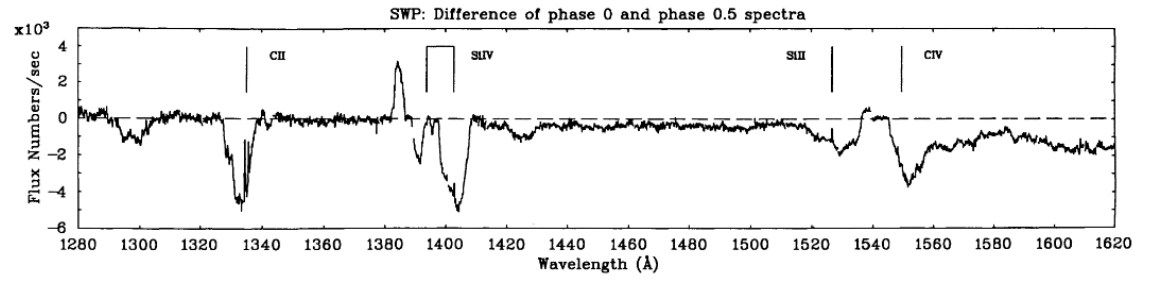
The radial dependence of the wind speed has important consequences, as it controls the steadystate density structure, and creates the diagnostically significant mapping from observable Doppler shift to radial location. In optically thick outflows such as those of WR stars, the detailed wind structure is even more important, because the hydrostatic surface of the star is hidden from view, leaving the wind as the only layer of the star that is directly accessible to observation. Dense winds also experience additional opacity changes as the temperature drops significantly and the radiation field shifts from being highly diffusive in deep layers to more free streaming in outer layers. Therefore, we wish to test the hypothesis that the different character of radiative transport and opacity gradients in denser winds, compared to less dense winds, changes the nature of the acceleration as a function of radius. This paper describes how this test can be carried out in a special sample of colliding-wind binary systems.

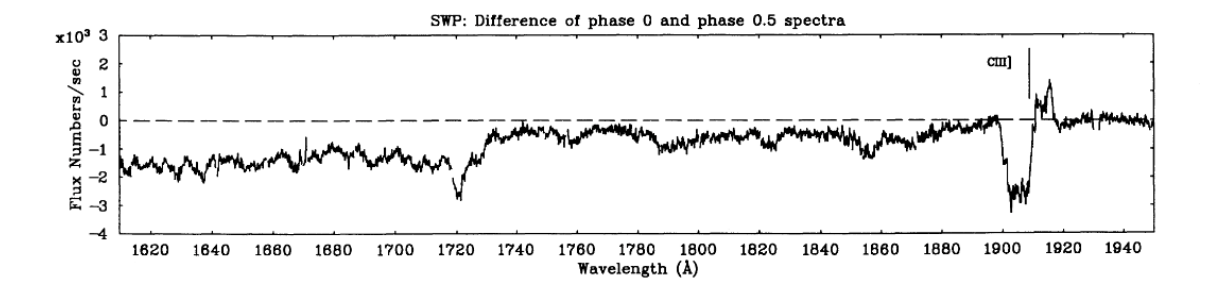
### 1.2 Making Use of Massive Stars in Binaries

Massive stars in binaries offer a unique opportunity to improve our understanding of radiatively driven winds. We can use the light from one star to probe the wind of the other star, allowing us to study the structure of its wind, which provides information on its density, the velocity law, the acceleration zone, and the ionization structure. This method has long been successfully used in the past to investigate, for example, the nature of WR stars (St-Louis et al, 1993).

An even older version of this approach that focused on light curves (Cherepashchuk et al, 1984) from the WN5 + O6 V eclipsing binary V444 Cygni, covering the wavelength range from  $\sim 2400\,\text{Å}$  to  $3.5\,\mu m$ , demonstrated that the WN5 star was hot (90,000 K), compact  $(r(\tau=1)=2.9\,R_\odot)$ , and had an outflowing atmosphere in which the temperature decreased smoothly with height. This helped resolve a long-standing controversy in the nature of Wolf-Rayet stars. Additional studies have investigated the stratification in the atmosphere (e.g., Eaton et al, 1985; Brown and Shore, 1986), and revealed, for example that Fe V in the wind of the WR star contributed to the atmospheric eclipse signal in the UV.







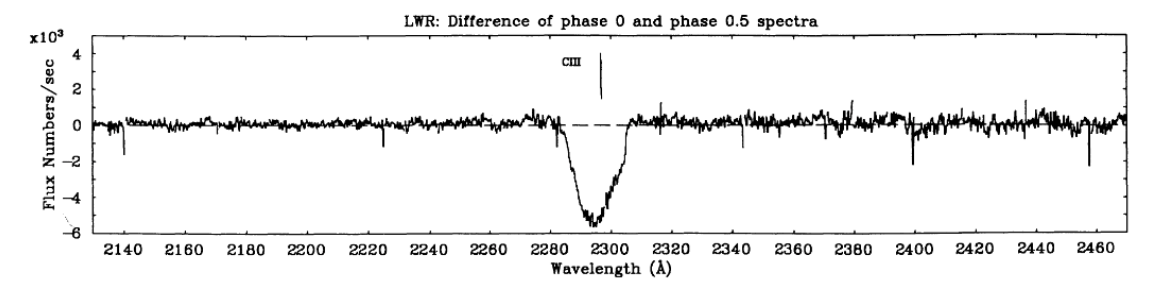


Fig. 1 Eclipse spectrum of  $\gamma$  Velorum. Figure 2 from St-Louis et al (1993). Reproduced with permission.

Koenigsberger and Auer (1985) used observations of 6 WR+O systems to show the extended WR atmosphere eclipsed the O stars, and used it to provide constraints on the atmosphere. A further analysis of four binaries by Koenigsberger (1990) showed that the Fe IV/Fe V ratio decreased with radius, and that the wind was still being accelerated at  $14 R_{\odot}$ . Auer and Koenigsberger (1994a) completed a detailed study and showed how line profile variations could be used to investigate the structure of the winds. Thus, select binary systems have a history of generating breakthrough studies of hot stars, a spirit that is extended into the present in this paper.

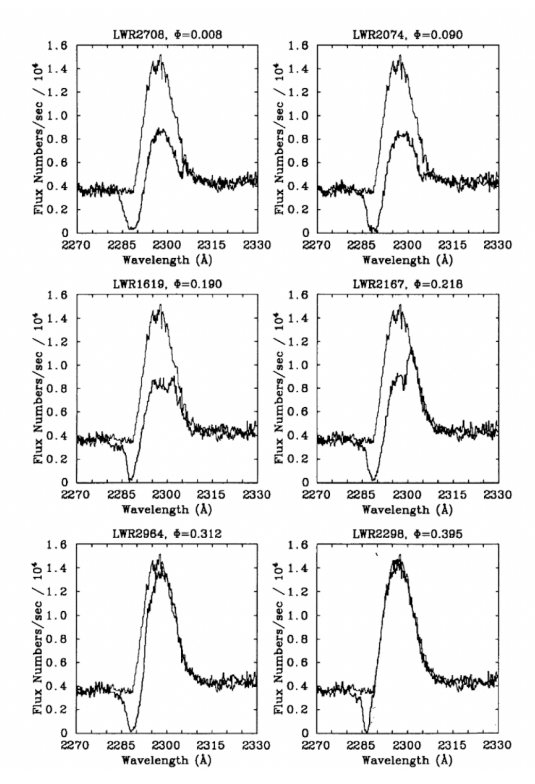


Fig. 2 Variations in the C III  $\lambda$  2297 profile with orbital phase. The thin line is the LWR 1316 ( $\Phi = 0.534$ ), and the thick line is the spectrum and phase indicated at the top of each graph. Figure 4 from St-Louis et al (1993). Reproduced with permission.

# 1.3 The Diagnostic Potential of Wind Eclipses

For a given binary configuration, spectroscopic variations are caused by the absorption of the light from one star by the atoms in the wind of the other. Previous UV spectroscopy has shown that absorption occurs mainly in low-excitation and resonance transitions of abundant ions (e.g. Koenigsberger and Auer, 1985). Therefore, these were called *selective wind eclipses*. As shown in Figure 1, for the WR+O binary  $\gamma$  Velorum (St-Louis et al, 1993), many ions show a symmetric absorption profile spanning positive and negative velocities in the difference spectrum between phases 0 (WR star in front) and 0.5 (O star in front), as expected. However, note that for certain lines, such as the semi-forbidden C III]  $\lambda 1909$  line and the entire forest of Fe IV lines, only absorption at negative velocities (towards observer) is observed. This unexpected behaviour still remains to be explained.

Examination of the times series for the same star of lines that behave more as expected has shown that the absorption profile is widest when the O companion is directly behind the WR star (called phase 0), and becomes narrower as it orbits to a perpendicular direction with the line-of-sight (phase 0.5). This is seen in Figure 2) by considering the difference between the line profile at the phase shown for the well-isolated C III  $\lambda$  2297 line, and that line seen when the O companion is nearly perpendicular to the WR star. Here there is evidence of wind eclipse when the O star is seen through the WR wind, at both red and blue Doppler shifts, spanning the range of projected velocities in the WR wind.

The detailed shape of the eclipse profile in the various transitions will be determined by the opacity encountered by the light from the companion star on its way to the observer and therefore on the projected velocity and ion abundance. As the companion moves through its orbit, different parts of the wind are probed as the line-of-sight differs for different configurations. This allows to probe different regions of the flow as a function of distance from the center of the star. If the two stars have strong winds, each one can act as a probe for the wind of the other. The combination of all resulting eclipse profiles observed at each position of the orbit contains information on the velocity, density and abundance structures of the winds.

Because of the presence of strong resonance lines of several abundant ions (e.g., due to Civ, Si IV), far ultraviolet spectroscopy is an ideal tool to study massive-star winds and particularly the spectroscopic variations originating from selective wind eclipse. Emission at any given frequency probes a large volume of the wind whereas absorption features primarily probes material along the line of sight to the star. The shape of the continuum light-curve over the binary orbit also allows to probe the column depth of the wind. The opacity of O and WR star winds at optical and UV wavelengths is primarily due to electron opacity. In WR stars Fe lines in the UV create a pseudo"continuum", and these also contribute significantly to the opacity.

In Figure 3 we illustrate the location at which a radial optical depth of 2/3 occurs as a function of wavelength for an O star and a WR star. The minimum radius, at these wavelengths, is set by electron scattering. At other wavelengths we

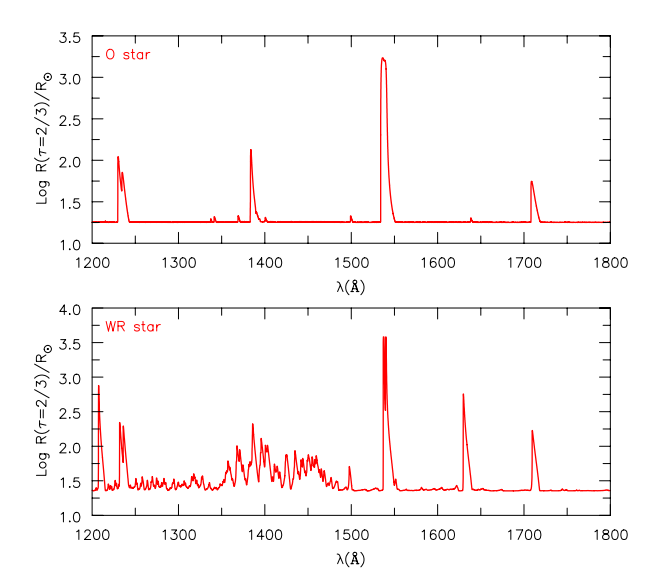


Fig. 3 Illustration of the location of where a radial optical depth of  $\tau=2/3$  occurs as a function of wavelength for an O-type and W-R type star.

see the influence of strong bound-bound transitions. The Fe forest is particularly prevalent in the WR star. While the actual numerical values are dependent on the adopted stellar radius, effective temperature and mass-loss rate, the plots do show how different wavelengths have the potential to be used as diagnostic probes in binary star systems.

### 1.4 Colliding Winds in Massive Binaries

Another aspect of close massive binaries is that the winds of the two stars collide forming a shock-cone structure, generating an asymmetric gas distribution. Colliding-wind binaries (CWB) can teach us a great deal about the individual stars and their winds because the geometry of the interaction region is strongly dependent on the component winds. Indeed, the details of the geometry and physical characteristics of the shock structure depend on the physical parameters of the individual winds, such as the mass-loss rate and velocity structure, thereby providing a further probe of these parameters.

Early theories describing these binaries used momentum flux (e.g. Girard and Willson, 1987) and ram-pressure balance (e.g. Kallrath, 1991), or hydrodynamic models (e.g. Stevens et al, 1992), until Cantó et al (1996) produced a complete analytical description in the limit of rapid shock

cooling (see Section 3.2.2). Further work in the area has focused on hydrodynamic simulations (Pittard, 2009; Lamberts et al, 2011; MacLeod and Loeb, 2020) and predictions of line profiles in both optical (Luehrs, 1997; Ignace et al, 2009; Georgiev and Koenigsberger, 2004) and X-rays (Rauw et al, 2016; Mossoux and Rauw, 2021). The result of these models, combined with a number of phaseresolved observations (e.g. Williams et al, 1990; Tuthill et al, 1999; Rauw et al, 2001; Sana et al, 2001; Rauw et al, 2002; Sana et al, 2008; Gosset et al. 2009; Parkin et al. 2009; Williams et al. 2009; Kennedy et al, 2010; Lomax et al, 2015; Nazé et al, 2018; Williams, 2019; Callingham et al, 2020), is that we have a good understanding of the expected geometry of colliding winds.

However, collision of the winds will additionally induce complex geometric structures that must be carefully analyzed to be able to extract the desired diagnostics. In this context, purely spectroscopic information may not suffice to resolve the potential ambiguities in such a complex structure, including the location and density of the bow shock, the inclination of the orbit, and the potential for asphericity in the intrinsic winds.

Polarimetric observations are thus a vital tool for revealing details of the mass-loss and masstransfer structures in these binaries. Both continuum emission (arising from the stars) and line emission (arising from winds, CIRs, or other shock regions) may be polarized in a CWB system via scattering from wind clumps (Harries et al, 1998; Davies et al, 2005), accretion disks (Hoffman et al, 1998), jets (Fox and Hines, 1998), bow shocks (Shrestha et al, 2018, 2021), and other asymmetric distributions of material or velocities within the system (Schulte-Ladbeck et al, 1992; Villar-Sbaffi et al, 2005; Fullard et al, 2020). Because scattering near the orbital plane tends to produce repeatable effects over many binary cycles, spectropolarimetric monitoring allows us to reconstruct the 3-D shapes of the regions scattering both continuum and line emission (e.g., St-Louis et al 1993; Lomax et al 2015; Fullard et al 2020).

Given that massive star winds are strongly ionized, it is reasonable to consider Thomson scattering as the dominant scattering method for photons in the winds, which in turn can polarize the observed light. The resulting polarization is sensitive to the geometry of scattering regions but also depends on the chemical composition

of the wind and its stratification as this will strongly affect the number of available scatterers. Therefore modeling polarimetric observations is a powerful tool to inform us about the geometry and density structures of the colliding winds in interacting systems. This information is critical to our understanding of the roles of binary stars in enriching the ISM and producing explosive transients and gravitational-wave sources.

The classic model approximates the timevarying continuum polarization caused by the illumination of stellar winds in a binary system viewed at an arbitrary inclination angle. In this model, the scattering region is described as an optically thin electron gas. The envelope pattern is assumed to co-rotate with the illumination sources, appropriate for steady-state systems in circular orbit. The illuminators consist of one point source at the center of the scattering region and an additional external point source representing the companion.

Brown et al (1982) extended the classic model developed by Brown et al (1978) (hereafter BME) describing the variation of continuum polarization from the illumination of circumstellar material in a circular binary to consider elliptical orbits, and Fox (1994) further extended the formalism to consider finite illuminators. Fox (1994) showed that occultation is only important in very close binary systems, where separation is less than 10 times the radius of the primary. Hoffman et al (2003) quantified the polarization produced by external illumination of a disk in a binary system. However, none of these enhancements to the theory included the effects of colliding winds in the time-dependent polarization results. St-Louis et al (1993) and Kurosawa et al (2002) modeled the polarization variations in the colliding-wind system V444 Cyg. Also, spectroscopic analysis of wind eclipses in general and for this system in particular have been carried out (Auer and Koenigsberger, 1994b), but the results have not been compared across a range of binary parameters to extract the important trends. Harries et al (2000) used a Monte Carlo formalism to estimate the polarisation caused by the scattering off dust and electrons in a colliding-wind shock cone if it were present in the long-period binary WR137 and found that for such a wide binary, the level would be very small (0.03%). Notwithstanding

these individual efforts, a general formalism has not yet been produced.

The *Polstar* team includes several experts in polarimetric modeling who will focus on developing the necessary tools to derive physical results from spectropolarimetric signatures. Polarization simulations of bow shocks, which polarize light both when illuminated by a central source and when the light originates within the shock itself (Shrestha et al, 2018, 2021), can be incorporated into binary models, as we discuss below. We will also investigate the effects of the wind collision regions and the distributed nature of line emission on the wavelength dependence of polarization. Given that complex continuum and line polarization signals associated with CWBs have been observed in several systems (St-Louis et al, 1993; Lomax et al, 2015; Fullard et al, 2020) and are likely to occur in the UV as well (Schulte-Ladbeck et al, 1992; Hoffman et al, 1998), such modeling efforts are critically important.

We intend to use *Polstar* to secure extensive UV spectropolarimetric timeseries of key massive binary systems in crucial lines with observations well-distributed around the orbital cycle. Having multiple diagnostics is important – different diagnostics probe different regions of the flow and trace different physics. For example, P Cygni absorption (blue shifted absorption associated with a redshifted emission profile) only samples material along our line of sight. Conversely, the emission line samples a much large volume. Continuum polarization, to some extent, is influenced by the whole volume. Optical studies do not have the necessary lines for the studies proposed here. A well-distributed time series is also crucial, since spectra taken at different times probe distinct orientations of the binary system. The combination of polarimetry and UV spectroscopy, almost unexplored, offers a unique opportunity to resolve ambiguities left by either approach alone. For example, the rate of change of the polarization position angle caused by the colliding wind interaction is a diagnostic of the orbital inclination that is complementary to light-curve considerations.

### 1.5 Small and Large-Scale Structure in Radiatively-Driven Winds

Growing observational evidence suggests that radiatively driven outflows are highly clumped,

7

naries

including the telltale presence of small sub-peaks observed to move from the center to the edges of strong emission lines in both O stars (e.g., Eversberg et al, 1998) and Wolf-Rayet (WR) stars (e.g., Lépine and Moffat, 1999). Inconsistencies in line strengths (e.g., Hillier et al, 2003; Crowther et al, 2002; Massa et al, 2003; Fullerton et al, 2006) and the relative strength of electron scattering wings to their adjacent profiles (e.g. Hillier, 1991; Hamann and Koesterke, 1998) also indicate that the winds are clumped. Large-scale structures are also thought to be present in the winds of most, if not all, OB stars, as shown by the presence of NACs and DACs in their ultraviolet spectra (e.g., Howarth and Prinja, 1989; Kaper et al, 1996) that are thought to be the observational signature of Corotating Interaction Regions (CIRs, Cranmer and Owocki, 1996; Mullan, 1986).

These important structural effects (Gayley et al, 2022) but can be further elucidated by the special diagnostics available in colliding-wind binaries. Small and large-scale wind structures change the density structure of the winds, and this influences the nature of the wind acceleration being probed in this paper. Further, winds may be porous both spatially (porosity) and in velocity space (called *vorosity*; Oskinova et al, 2007; Owocki, 2008). Spatial porosity affects both line and continuum radiation transfer whereas vorosity, which refers to gaps in velocity space, only effects line transfer. These phenomena lead to uncertainties in derived parameters such as massloss rates, luminosities, radii, and abundances. In turn, this limits our ability to place accurate constraints on stellar and galactic evolution. As will be seen below, two very bright systems ( $\gamma$  Velorum and  $\delta$  Ori) that will be targeted for close examination for clumping effects are also targeted here by virtue of their binary status, and these systems will be especially informative when the Polstar diagnostics utilized in the two objectives are combined.

### 1.6 Mass-loss rates

Mass-loss rates included in stellar evolution calculations typically use a fitting law with an adjustable parameter (e.g. MESA or Geneva code, Paxton et al, 2011; Meynet et al, 2015). These laws are based on a combination of theoretical and observational studies of mass loss in O stars.

For radiatively-driven winds of hot stars, the theoretical mass-loss rates of Vink et al (2001) and Nugis and Lamers (2000) are typically adopted. For more luminous stars, they are in rough agreement (factor of two) with empirically derived mass-loss rates, but for late O stars the rates can differ by an order of magnitude. Even a factor of two uncertainty is a significant problem for understanding how massive stars evolve and effect their environment.

Observational mass-loss rates are generally derived using an empirical velocity law, and by necessity one is forced to make assumptions regarding the inhomogeneity of the wind (e.g., Hillier et al, 2003; Bouret et al, 2012; Sander et al, 2012; Shenar et al, 2015). Typically, the wind is assumed to be clumped, with a fraction f occupied by the clumps. Porosity is generally ignored, and the interclump medium is assumed to be void. To first order, empirical modeling derives  $\dot{M}/\sqrt{f}$ . Constraints on f can be placed by using the strength of electron scattering wings in WR stars, and by using P Cygni profiles in O stars. The latter, however, is more uncertain because of the effects of porosity and vorosity.

Current radiative transfer codes can, potentially, derive the velocity law and mass-loss rates from first principles (e.g., Vink et al, 2001; Sander et al, 2020; Björklund et al, 2021; Vink and Sander, 2021). However such codes make assumptions about clumping, and may use approximate radiation transfer techniques such as the use of the Sobolev approximation (Sobolev, 1960). Further, there are still uncertainties about the nature and role of microturbulence at the sonic point (Hillier et al, 2003; Lucy, 2007), and the role of inflation, convection and density inhomogeneities in optically thick regions of the flow (e.g., Ishii et al, 1999; Petrovic et al, 2006; Cantiello et al, 2009; Gräfener et al, 2012; Grassitelli et al, 2016). Finally there are uncertainties in the atomic data.

As a consequence of these uncertainties, spectra derived from models constructed on first principle generally do not provide a good fit to observed spectra. At best, mass-loss rates must be regarded as uncertain to at least a factor of two, and in some cases the uncertainty is much larger. However, a factor of two variation in mass-loss rate can have a strong influence on a star's evolution. This is seen in theoretical calculations

(e.g., Maeder, 1981), and is likely illustrated by the different massive star populations in the LMC and Galaxy, as line-driven mass-loss rates depend strongly on metallicity (e.g. Vink et al, 2001). Accurate mass-loss rates require an understanding of the density structure, which connects to the velocity structure and the physics of wind driving. Thus the objective considered in this paper is also relevant to establishing more accurate mass-loss rates in specially selected systems, using the unique diagnostics available in these binary systems.

### 2 PolStar Capabilities and Data Products

Using Polstar (Scowen et al, 2022), we intend to probe the details of the wind density of the stars in these systems by using the light from the other star as a probe. Because the presence of two stars with strong winds in a binary generally leads to the formation of a shock-cone structure, we must also take this into account and actually we intend to use it to further constrain the physical characteristics of the outflows. Finally, companion stars are also not independent light sources - their radiation field can modify the wind of the other star, and in close binaries one or both winds may not reach terminal speed either because of the collision or because of the companion's radiation field. Radiative braking, the deceleration of one wind by the radiation field of the secondary, will modify the location and structure of the bow shock. The combination of UV spectroscopic time series, polarimetric observations, and spectra modeling will ultimately allow us to constrain the mass-loss rates to unprecedented accuracy.

Phase-dependent observations of systems with elliptical orbits or with different separations will allow us to investigate how the radiation field of one star influences the wind of the second star. Our strategy to address these questions is to study a wide range of wind densities in binary systems with high enough inclination and short enough periods for the companion light to be seen deeply through the primary wind. For the brighter stars, we intend to obtain a full phase coverage of ultraviolet spectropolarimetric observations for each system at the highest possible spectral resolution. Depending on the brightness of a given target,

we can bin the spectral resolution as necessary to secure sufficiently high quality signal-to-noise to identify telltale spectral features and polarization variability, with good phase coverage.

We have identified a sample of 20 massive binary systems for which there is evidence in the literature of the presence of a colliding wind structure, and which can be observed with Polstar. These are listed in Table 1.

### 2.1 Spectroscopic Experimental Design

In order to monitor the spectroscopic variability caused by selective wind eclipses and the presence of a colliding wind shock cone and to capture all the subtleties of the phase-related changes, we will use Polstar to secure a series of 10 high-resolution spectra, well-distributed over the orbital phase of each binary on our target list. We plan to observe the 8 brightest systems at the highest resolution (R=30000), the 6 next bright binaries at a slightly lower resolution (R=20000) and finally the 6 less UV bright targets at a more moderate resolution (R=10000). Including fainter targets broadens our system parameters and allows us to include especially interesting targets with overlap with other Polstar objectives, such as V444 Cygni, a wellstudied WR eclipsing binary, HD5980, for which one component star has recently undergone an LBV-type eruption, WR 69, a system including a WC9 type star that produces dust, and WR 137, a rare system consisting of a WR star and an Oe star (with a decretion disk) in a wide orbit.

For the three brightest targets, we require a signal-to-noise ratio (SNR) of 3000 to reach the necessary high polarimetric precision, while also achieving the high spectral resolution needed to detect the details of the selective wind absorption profile, and details of the clumpy nature of the winds and of the colliding-wind shock-cone. For the other systems, we aim for a SNR of 100 (already 5-6 times higher that what is currently available from IUE data), which will still provide excellent quality data. We plan to use the knowledge gained with our test systems to enhance the interpretation of the lower SNR observations.

Table 1 Target list

| Star  | HD number   | Туре   | Period (d)  | V   | UV Flux*  | Ch. 1†<br>exp time(s)                            | Ch.2†<br>exp time(s)                             |
|---|---|--|---|---|---|--|--|
| Ch.1 spec., N=1<br>and polar. (SNR=3000)<br>Gamma Velorum<br>Delta Ori<br>29 CMa                                | 68273<br>36486<br>57060                               | WC8+O7.5III-V<br>O9.5II+BO5.III<br>O7Iaf+O9  | 78.05<br>5.7<br>4.4                                 | 1.83<br>2.41<br>4.95                        | 263<br>147<br>7.5                               | 2000<br>3550<br>70200                            | 60<br>60<br>60                                   |
| Ch.1 spec., N=1 (SNR=100)<br>Ch. 2 polar. (SNR=3000)<br>Plaskett<br>WR22<br>WR79                                | 47129<br>92740<br>152248<br>152270<br>149404          | 07.51+061<br>WN7h+09III-V<br>07.5III(f)+07III(f)<br>WC7+05-8<br>07.5If+0N9.7I        | 14.4<br>80<br>5.8<br>8.89<br>9.8                    | 6.06<br>7.16<br>6.05<br>6.95<br>5.52        | 1<br>1.1<br>0.8<br>0.5<br>0.5                   | 600<br>510<br>720<br>1150<br>1150                | 1840<br>1680<br>2300<br>3680<br>3680             |
| Ch.1 spec., N=1.5 (SNR=100)<br>Ch. 2 polar. (SNR=3000)<br>WR133<br>WR42<br>Eta Car(2020)<br>WR 25<br>WR140      | 190918<br>97142<br>93308B<br>93162<br>193793<br>93205 | WN50+09I<br>WC7+05-8<br>LBV<br>O2.51f*/WN6+O<br>WC7pd + O5.5fc<br>O3.5 V((f)) + O8 V | 112.8<br>7.886<br>2022.7<br>208<br>2895.0<br>6.0803 | 6.7<br>8.25<br>6.21<br>8.84<br>6.85<br>7.75 | 0.35<br>0.22<br>0.2<br>0.13<br>0.1<br>0.1       | 1110<br>1800<br>1950<br>4020<br>4020<br>6300     | 585<br>930<br>1050<br>1590<br>2100<br>2100       |
| Ch.1 spec., N=3 (SNR=100)<br>Ch. 2 polar. (SNR=1000)<br>WR137<br>HD5980<br>V444 Cygni<br>WR699<br>WR127<br>WR21 | 192641<br>5980<br>193576<br>136488<br>186943<br>90657 | WC7+O9e<br>WN4+O7I<br>WN5+O6II-V<br>WC9d+OB<br>WN3b+O9.5V<br>WN5o+O4-6               | 4766<br>19.3<br>4.21<br>2.293<br>9.555<br>8.25443   | 8.15<br>11.31<br>8<br>9.43<br>10.33<br>9,76 | 0.04<br>0.04<br>0.02<br>0.015<br>0.012<br>0.011 | 5100<br>5100<br>11100<br>15600<br>21400<br>22800 | 5100<br>5100<br>11000<br>13680<br>17160<br>18720 |

\*UV Flux at 1550A (10<sup>-10</sup> erg/s/cm<sup>2</sup>/Å) † at 1500Å, D=60 cm, R=30000/N for spectroscopy

## 2.2 Polarimetric Experimental Design

We have selected three massive binaries that are bright in the ultraviolet to observe at the very highest spectroscopic resolution in spectropolarimetry to serve as test cases. These include hot, massive stars having reached different stages of evolution from bright giants to WR type. Although our standard polarization precision for this experiment is  $1 \times 10^{-3}$ , for these unusually bright systems, we aim for a SNR of 3000 in order to be able to detect the very faint polarization signals from the colliding wind shock-cone, down to a precision of  $5 \times 10^{-4}$ . We also plan to observe these targets in channel 2 at lower spectral resolution, and appropriately shorter exposures, in order to characterize the wavelength dependency of the polarization at similar precision. For the other binaries, our strategy is to obtain the highest SNR possible for the UV flux of the target (either 3000 or 1000) but at lower spectral resolution using observations in channel 2. Channel 1 observations at a lower SNR are also important to characterize the wavelength dependency of the polarization. For all polarization measurements of our targets, we will be able to remove the non time-variable but wavelength-dependent interstellar polarization vector from the interstellar medium between each target and the observer, using the method described elsewhere in this topical collection by Andersson et al.

### 3 Polarisation modeling

### 3.1 Linear Polarization Across Spectral Lines

At optical and UV wavelengths it is often a good approximation to assume that electron scattering is coherent in the frame of the electron. However, since the electron is moving (due to both thermal and large scale motions) relative to both the source and observer there will be a wavelength shift in the observer's frame (Auer and van Blerkom, 1972). Thermal motions can lead to either a decrease or increase in the scattered photon's wavelength, while scattering by an expanding monotonic flow will always lead to a redshift. These velocity shifts are observed — in P Cygni for example, in which the thermal

electron velocities are larger than the wind velocity, the Balmer series, among others, show nearly symmetric broad extended wings centered on the emission profile (Bernat and Lambert, 1978). By contrast, in the spectra of many WR stars only a red electron scattering wing is seen, since in these stars the wind velocities are larger than the electron thermal velocities (Hillier, 1984).

For continuum polarization the velocity shifts induced by electron scattering are generally unimportant. However, they are of crucial importance in understanding line polarization. In Fig. 4 we show an extreme example, taken from polarization studies of supernovae, where the line shift is crucial. In the Type II SN 2013ej the polarized spectrum is very similar to the observed spectrum (Leonard et al, 2021). However, it is different in two important ways: First, the spectrum is redshifted. Second, the agreement between the intrinsic and polarized spectrum depends on which spectral feature is being examined. Both effects are easily understood by assuming that the scattering source is offset from the SN emitting region, and by noting that line emission in a SN region is stratified (different lines originate in different regions of the SN ejecta). Dessart et al (2021) argued that the scattering region was due to a nickel bubble, with an enhanced electron density offset from the center of the ejecta. Due to motion relative to the source, the spectrum is shifted to the red. Furthermore, the similarity between the intrinsic and scattered light will generally be highest for lines arising in the interior regions of the SN ejecta, since in that case the scattering angle is the same, unlike the case where the emission is formed over a much larger volume.

When optically thin electron-scattering is assumed, and other absorption processes neglected (e.g., purely bound-bound transitions), models predict that for an oblate spheroid the polarization should be parallel to the major axis. The reason is simple – more photons will be scattered from the equatorial regions (with their electron vector parallel to the major axis) than the polar regions. However, when optical depth effects are allowed for, the polarization can flip sign, as scattered photons become more isotropic in the higher optical depth equatorial region.

The above scenario is illustrated in Fig. 5 where we present the spectrum for a WN Wolf-Rayet star assuming it has an oblate wind with

a polar to equatorial density ratio of 0.3. Near  $1800 \,\text{Å}$ , the polarization is positive, as expected for an oblate spheroid. However, around  $1400 \,\text{Å}$ , the polarization is negative, a consequence of Feblanketing, which increases the total opacity and also introduces line effects. The assumed axial symmetry guarantees that the position angle must be parallel or perpendicular to the rotation axis, so here we have taken the Stokes Q component to subtract light polarized perpendicular to the rotation axis from light polarized along the axis (and the U component at 45 degrees to that would be zero in this symmetry).

Both of the above examples illustrate how the polarization contains important information about the structure of circumstellar matter, whether it be a SN ejecta or a wind. Importantly, we now have the numerical tools to interpret these observations. Polarization, in conjunction with other observations provides an invaluable tool to help understand astrophysical objects, especially since most are spatially unresolved with modern telescopes.

### 3.2 Polarization from Colliding Wind Binaries

While the preceding section focused on the spectropolarimetric signatures that can arise from aspherical winds of single stars, here the focus is on binary stars. Whereas ? emphasize interacting binaries, we explore variable wavelength-dependent polarization from massive stars with colliding winds. The time dependence and wavelength dependence encode information about the geometry of the orbit (including viewing inclination that is important for obtaining accurate masses), the geometry of the bow shock, and properties of the respective stellar winds such as mass-loss rates.

### 3.2.1 Continuum Linear Polarization of Colliding Wind Systems

BME present a theoretical construction for thin electron scattering in generalized envelopes with an arbitrary number of illuminating point sources. The two main limitations of BME are in relation to finite star effects (e.g., occultation) and the explicit assumption of thin scattering. For application to binary stars, the former is often an

8

11

naries

Leonard et al

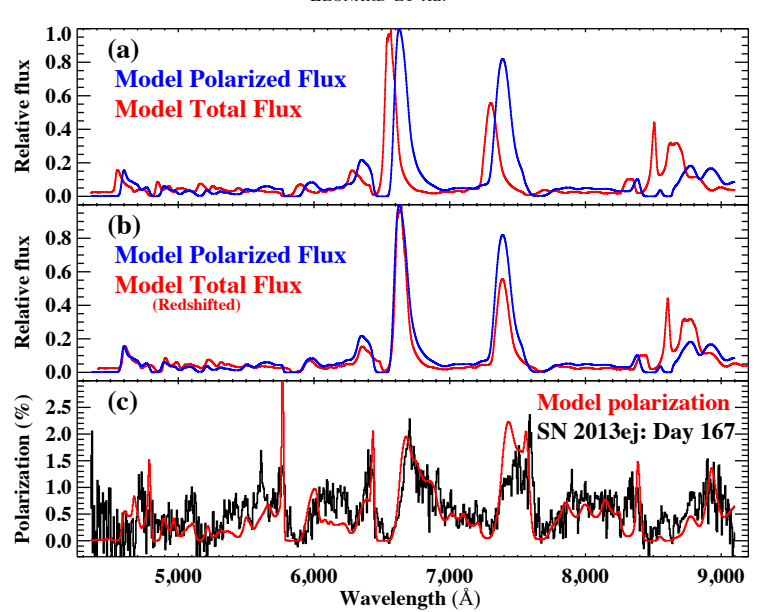


Fig. 4 Illustration of how velocity shifts influence the polarized spectrum. Top panel shows how the scattered spectrum (blue) is offset to the aschitem threaturement in the contained to the second in the contained the similarities between the two spectral-However (2000) ause spectrals deatures is an isopower landarged of yradii, the agreement is not perfect. The et al (2021). Reproduced with permission presented in a manner identical to that shown for the data of SN 2013ej in Figure 1, where we have again normalized all spectra to 1.0 at the location of the H $\alpha$  peak. (c) Direct comparison

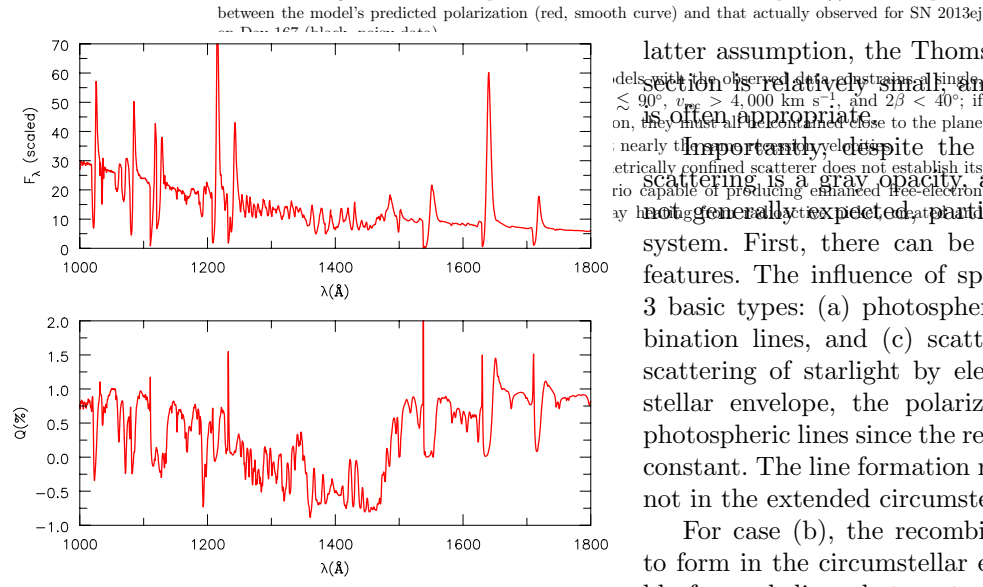


Fig. 5 The spectrum and polarization (Stokes Q) for a WR star with an oblate stellar wind viewed edge on. The ratio of the polar to equatorial density is 0.3. Notice how the polarization switches sign - a consequence of optical depth effects in the wind.

adequate assumption unless the binary separation is quite close or the system is eclipsing. For the

latter assumption, the Thomson scattering crossdels settion observed at ively trainfall in and so thin scattering  $\lesssim 90^{\circ}$ ,  $v_{\rm rec} > 4,000 \ {\rm km \ s^{-1}}$ , and  $2\beta < 40^{\circ}$ ; if on, they much all PRF in the close to the plane

nearly the portantly veldespite the fact that Thomson etrically confined scatterer does not establish its scattering is a gray opacity a flat polarization is rio capable of preducing enhanced free-electron. ay haotigenerally tiexpected at particularly for a binary system. First, there can be changes across line features. The influence of spectral lines come in 3 basic types: (a) photospheric lines, (b) recombination lines, and (c) scattering lines. For the scattering of starlight by electrons in a circumstellar envelope, the polarization is flat across photospheric lines since the relative polarization is constant. The line formation resides at the source, not in the extended circumstellar envelope.

For case (b), the recombination line is taken to form in the circumstellar envelope. It is possible for such line photons to be scattered by the circumstellar electrons. But such photons are not originating from the star but distributed throughout the envelope, and represent a diffuse source of photons for scattering. Variations in polarization can be complex. As an example, Ignace (2000a) explored variations in polarization at  $H\alpha$  in a Be star disk with a 1-armed spiral density wave: the polarization in the continuum is little affected

by the antisymmetric structure, but in  $H\alpha$  the density-squared emissivity leads to a highly non-symmetric radiation field in the disk. The result is distinct polarimetric behavior within the line as compared to the continuum. Similar consequences may apply to colliding wind systems (Fullard, 2020).

There is an important limiting scenario for case (b) known as the "line effect" (e.g., Schulte-Ladbeck et al, 1990). This is when the recombination line is formed at a large radius and the electron scattering occurs mainly over a more compact region close to the star. In this situation the line photons are little scattered, and strong line emission can contribute to the flux  $F_I$  but not  $F_Q$  or  $F_U$ . The result is a reduction in the relative polarization p (sometimes referred to as "diluted" polarization).

Case (c) refers to the possibility of scattering resonance lines as an additional polarigenic opacity. Although resonance scattering polarization for stellar winds has been explored in limited applications (Jeffery, 1989; Ignace, 2000b), the topic has lacked an observational driver. Such effects require a high-resolution UV spectropolarimeter and the computational tools for making predictions of effects and providing fits to data. The data have largely not existed, given that WUPPE was of lower spectral resolution. Polstar will provide new possibilities for case (c), and the team possesses the radiative transfer tools for developing diagnostics that combine both electron and resonance line scattering.

For hot stars in addition to the effects across lines are the chromatic effects in the relative polarization that arise simply from the presence of two stars with different temperatures in a binary. The net polarization from the unresolved binary systems involves a weighted linear sum of the polarized contributions from scattered starlight by each star. The net polarization is of the form:

$$p(\lambda) = \epsilon_1 p_1 + \epsilon_2 p_2,\tag{1}$$

where

$$\epsilon_1 = \frac{L_1(\lambda)}{L_1(\lambda) + L_2(\lambda)},\tag{2}$$

and

$$\epsilon_2 = \frac{L_2(\lambda)}{L_1(\lambda) + L_2(\lambda)},\tag{3}$$

and  $p_1$  and  $p_2$  represent the relative polarization caused strictly by geometric effects from the perspective of each separate star. These two parameters bracket the overall scale of the net polarization for an unresolved source. Neither are functions of wavelength; chromatic effects in the polarization arise from the luminosity weighting by the two stars.

To understand general expectations for  $p(\lambda)$ , it is helpful to consider limiting cases. If the temperatures of the two binary components are identical, the polarized spectrum will be flat at all wavelengths, in the absence of multiple scattering effects. If the stars have different temperatures, then the polarized spectrum,  $p(\lambda)$  will not in general be flat. In particular, for hot massive stars, the deviation from a flat polarized spectrum occurs mainly in the UV. Thinking simplistically in terms of Planckian stellar spectra, hot OB star spectra in the optical and longer wavelengths will be in the Rayleigh-Jeans regime. At such long wavelengths,  $p(\lambda)$  will be flat because both  $L_1$  and  $L_2$  have the same spectral shapes. It will be flat until bound-free or free-free emission becomes relevant. In particular, a WR star does not achieve the Rayleigh-Jeans limit at any wavelength owing to significant free-free and bound-free emission from the wind. By contrast at short wavelengths in the UV, where *Polstar* will operate, the presence of differing Wien peaks ensures that  $\epsilon_1$  and  $\epsilon_2$ vary with wavelength, and  $p(\lambda)$  will be chromatic. Formally,  $p(\lambda)$  is bounded by  $p_1$  and  $p_2$ , which provides a richer set of constraints for inferring the geometry of the system.

For our application to massive colliding wind binary systems, we assume that the colliding wind interface (CWI) is axisymmetric about the line-of-centers joining the two stars, following Cantó et al (1996). We further assume that the separate winds of the two stars are each spherically symmetric up to the CWI. The *Polstar* team possesses a suite of computational tools for time-dependent hydrodynamical simulation of colliding winds (e.g., Russell et al, 2017) and for the radiation transport for synthetic polarization spectra (Hoffman, 2007; Huk, 2017). Here we explore only the BME approach as the underlying assumptions can often be valid or nearly so.

#### 3.2.2 Model Prescription

Cantó et al (1996) present a convenient semianalytic bow shock model solution for the shock properties resulting from the collision of two spherical winds at terminal speed under the condition of strong radiative cooling<sup>1</sup>. In this model, the bow shock geometry and its surface density is determined by two fundamental ratios:

$$\beta = \frac{\dot{M}_2 v_2}{\dot{M}_1 v_1}, \text{ and} \tag{4}$$

$$\alpha = v_2/v_1, \tag{5}$$

where "1" and "2" refer to the two stars, v is the wind terminal speed, and  $\dot{M}$  is the mass-loss rate. We identify the primary as star #1 in such a way that the ratio of wind momenta is  $\beta \leq 1$ . By this convention the ratio of terminal speeds,  $\alpha$ , may be smaller, larger, or equal to unity. Note also that the primary by our definition may not be the most luminous star in the system for all (or any) wavelengths. The key outcomes of their solution is the location of the bowshock and its geometry, along with the surface density of material in the bow shock.

The individual winds are taken to be spherical at terminal speed with densities varying with the inverse square of the distance from the star. The semi-analytic solution of Cantó et al (1996) yields the geometry of the bowshock in terms of distances, R, from the secondary and the primary stars as (refer to Fig. 6 for a schematic):

$$R_{2,S} = D \frac{\sin \theta_1}{\sin(\theta_1 + \theta_2)}, \text{ and } (6)$$

$$R_{1,S} = \sqrt{D^2 + R_{2,S}^2 - 2 D R_{2,S} \cos \theta_1}, \quad (7)$$

where D is the separation between the two stars at any moment. Naturally the solution is only valid when  $D > R_{2,*}$ . A special quantity is the standoff radius of the bowshock along the line centers, denoted as  $R_{1,0}$  and  $R_{2,0}$ , given by

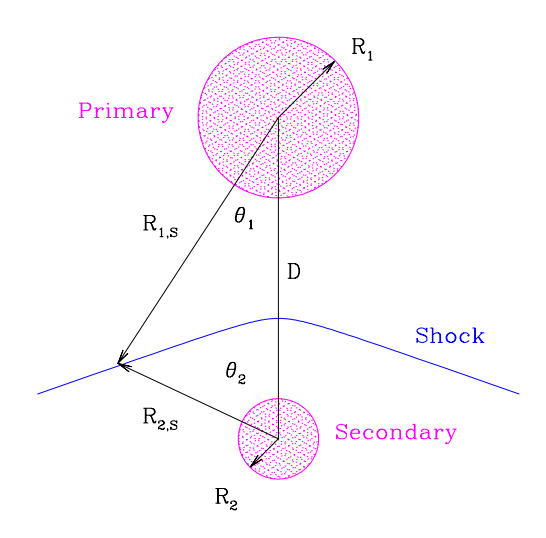


Fig. 6 Top-down illustration of the two stars (primary as "1" and secondary as "2") and the bowshock formed by the colliding winds. Labeled variables are defined in text. (Figure similar to one in Ignace et al, 2022)

$$R_{2,0} = \frac{\beta^{1/2}}{1 + \beta^{1/2}} D$$
, and (8)

$$R_{1,0} = \frac{1}{1 + \beta^{1/2}} D. \tag{9}$$

The case  $\beta = 1$  corresponds to a planar shock between identical stars and winds, with  $\theta_{1,\infty}$  =  $\theta_{2,\infty} = \pi/2$ . The parameters  $p_1$  and  $p_2$  are set by the binary orbital separation D, the wind properties, and the viewing inclination. For a circular orbit, D is fixed and so are  $p_1$  and  $p_2$ . Yet there can be time dependence of the polarization and position angle with orbital phase that arises as the stars orbit each other (c.f., BME). If the orbit is eccentric, then separation D is a function of orbital phase as well. The calculation of  $p_1$  and  $p_2$ is detailed in Ignace et al (2022).

#### 3.2.3 Model Results

For illustration, we use the approach of Ignace et al (2022), and evaluate synthetic spectra with linear polarization for a binary involving a WR star and an O star. For SEDs we use the online

<sup>&</sup>lt;sup>1</sup>Some colliding wind shocks are better described by adiabatic cooling (e.g., Gayley, 2009). For our purposes the solution of Cantó et al (1996) is convenient for its simplicity and for overall characterization of the issues involved for polarimetric variability.

 ${\bf Table~2~Stellar~and~Wind~Parameters~for~Colliding~Wind~Polarization} \\$ 

|  | WN5/6 | O7V   |
|--|-------|-------|
| T (kK)                                       | 56.2  | 36.0  |
| $\log L/L_{\odot}$                           | 5.30  | 5.01  |
| $\log \dot{M} \ (M_{\odot} \ {\rm yr}^{-1})$ | -5.13 | -7.00 |
| $v_{\infty} \; (\mathrm{km/s})$              | 1600  | 2710  |
| $R_*/R_{\odot}$                              | 4.7   | 8.2   |
| $M_*/M_{\odot}$                              | 25    | 25    |

PoWR model grid<sup>2</sup> (Gräfener et al, 2002; Sander et al, 2015; Hainich et al, 2019). For the WR spectrum, we selected model 08-10 from the Milky Way WNE models. For the O star, we used model 36-40 at Galactic metallicity. Table 2 lists the stellar and wind parameters.

Figure 7 shows values of  $p_1 = p_{WR}$  (blue) and  $p_2 = p_O$  (red) in percentage for these example stellar and wind parameters plotted with binary separation D in solar radii. The parameter  $p_O < 0$ , so its negative is plotted. For the WR star, its wind is far stronger than the O star, so the bow shock is located far from the WR component and close to the O component. As a result,  $p_{WR} \ll -p_O$  and so it is plotted at  $5\times$  its value for ease of viewing. Also shown are dotted lines that scale as  $D^{-1}$  for binary separation. The parameter  $p_{WR}$  closely follows that trend, whereas  $p_O$  follows it only at larger separations. But even at relatively close separations, the trend of  $p_O$  is close to  $D^{-1}$ .

The PoWR model spectra are plotted in the upper left panel of Figure 8, with magenta for the WR component, blue for the O component, and black for the summed spectrum. Note that the total spectrum is normalized to have unity peak flux. The upper right panel includes interstellar extinction at a value of  $A_V = 2$ . Ignoring the "blue bump" (Cardelli et al, 1989), we use an extinction law of  $A_{\lambda} = A_{V}(0.5 - 1.07\lambda_{\mu}),$ where the wavelength is in microns. While ignoring the blue bump fails to properly characterize the expected observed spectrum, it does not affect the effect of interstellar polarization described by the Serkowski Law (Clayton and Mathis, 1988; Martin et al, 1999), which displays no blue bump features.

At lower left of Figure 8 is the polarized spectrum without interstellar polarization using

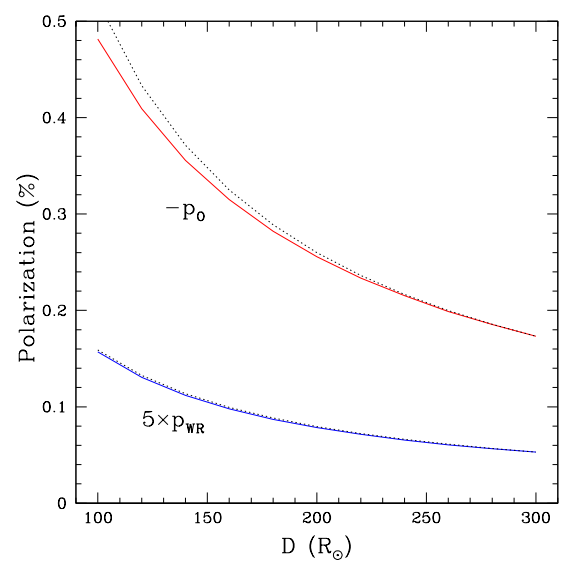


Fig. 7 Plot of  $p_{WR}=p_1$  and  $p_O=p_2$  for a WR+O binary using the Cantó et al (1996) bow shock solution against binary separation D in  $R_{\odot}$ . Stellar and wind parameters are given in the text. With  $p_O<0$ , the negative of its value is plotted (red). With  $p_{WR}\ll -p_O$ , the value has been increased by  $5\times$  for ease of viewing (blue). The dotted lines are  $D^{-1}$  curves showing that  $p_{WR}$  closely follows this trend for all separations, whereas  $p_O$  approaches it for wider separations.

 $p_{WR} = +0.0202$  and  $p_0 = -0.32$  for a binary separation of  $D = 160R_{\odot}$  from Figure 7. Note that for the masses of Table 2, the orbital period for this illustrative example would be about 45 days. We have oriented the system as pole-on and with all the polarization in Stokes-Q.

There are several key features regarding this figure. First, whenever the WR flux dominates, the polarization is positive and close to zero. This is evident around EUV wavelengths. Whenever the polarization is significantly negative, the O star tends to dominate. This occurs from the FUV through the optical. For IR wavelengths, the net polarization reduces as the free-free continuum of the WR component gradually gains in brightness over the O star. Also notable is that the polarization may become larger or smaller across lines, depending on whether a strong line belongs to the WR or O star component.

At lower right is the stellar polarization with interstellar polarization from a Serkowski Law now included. The Serkowski Law is given by

 $<sup>^2</sup> www.astro.physik.uni-potsdam.de/ \\ wrh/PoWR/powr-grid1.php$ 

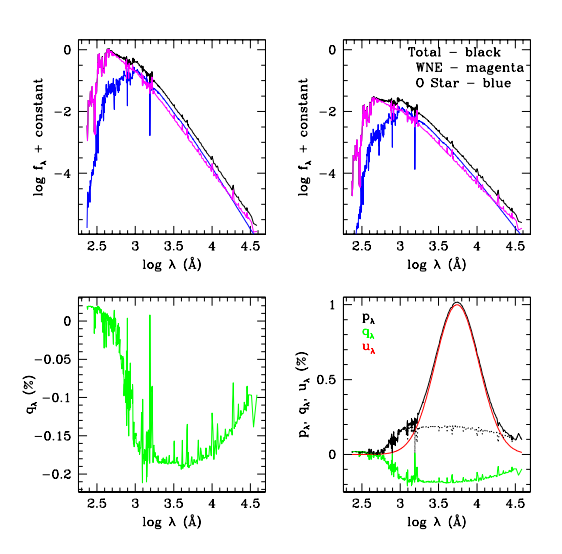
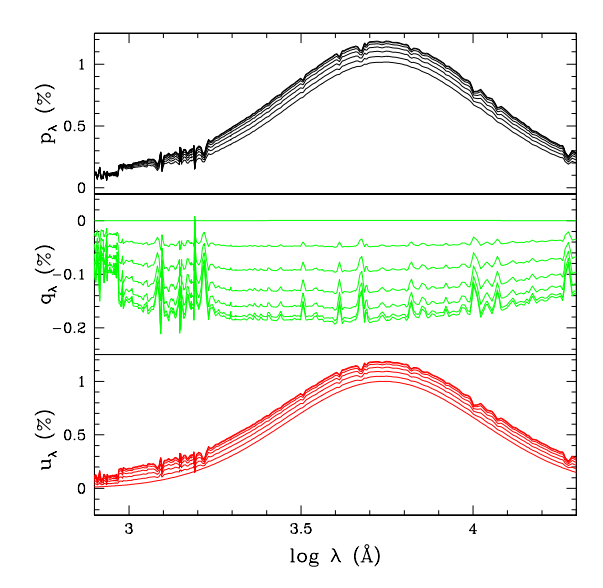


Fig. 8 (Upper left) The spectral energy distributions of the WR star (magenta), O star (blue), and combined (black). (Upper right) The spectra from the upper left panel now with interstellar extinction included as described in the text. (Lower left) The intrinsic polarization spectrum from the binary entirely in  $q_{\lambda}$ , as described in the text. (Lower right) The polarized spectrum now including a Serkowski Law as described in the text. Here  $q_{\lambda}$  in green is entirely stellar;  $u_{\lambda}$  in red is entirely interstellar;  $p_{\lambda}$  in black is the total polarization; and the dotted black line is  $p_{\lambda} = \sqrt{q_{\lambda}^2}$  if there had been no interstellar polarization.

$$p_{ISM}(\lambda) = p_{\text{max}} \exp \left[ -K \ln(\lambda/\lambda_{\text{max}})^2 \right], \quad (10)$$

where  $p_{\text{max}}$  is the peak polarization for which we choose 1%, K has a typical value of 1.15, and  $\lambda_{\text{max}}$  is the wavelength of the peak interstellar polarization, which has a typical value of 550 nm. We orient the polarization at a position angle so it is entirely in Stokes-U. The lower right panel shows  $q_{\lambda}$  in green (same as shown in the lower left panel), which is entirely stellar,  $u_{\lambda}$  which is entirely interstellar,  $p_{\lambda} = \sqrt{q_{\lambda}^2 + u_{\lambda}^2}$  in black, and then  $q_{\lambda}$  as the dotted black line. Interstellar polarization strongly affects the polarization in the optical band, whereas the stellar polarization becomes dominant toward UV and IR wavelengths.



**Fig. 9** The three panels display total polarization (top), Stokes-Q (middle), and Stokes-U (bottom) for half a binary orbit as seen pole-on. Interstellar polarization is entirely in  $u_{\lambda}$ , whereas the stellar polarization smoothly varies between  $q_{\lambda}$  and  $u_{\lambda}$  owing to the changing orientation on the sky.

Figure 9 displays the results of Figure 8 for different polarization position angles assuming a circular orbit and a pole-on view. The upper panel is the total polarization; middle is for Stokes-Q; and bottom is for Stokes-U. Note that the scale for the lower panel differs from the other two. With our arrangement of the interstellar polarization position angle, the modulation of  $q_{\lambda}$  with orbital phase is entirely stellar. By contrast,  $u_{\lambda}$  is a blend of stellar and interstellar. The variations are displayed for only half the orbit for which  $q_{\lambda} \leq 0$ .

For analysis of observational data, it is important to note that the polarization position angle for the interstellar component is fixed and unvarying with time. Thus, if a binary system were strictly axisymmetric, there would be a position angle for which the Stokes  $q_{\lambda}$  and  $u_{\lambda}$  could be rotated to eliminate (through fitting) the Serkowski Law from infuencing one of these Stokes parameters, such as  $u_{\lambda}$  in our illustrative example. In this case the influence of interstellar polarization would be relegated entirely to  $q_{\lambda}$ . However, if the stellar system is not strictly axisymmetric, then there is no rotation of the observed Stokes-Q and U components in which the stellar polarization can be isolated to a single Stokes

parameter, with the interstellar contribution limited to the other. The interstellar polarization can still be eliminated through analysis of the  $q_{\lambda}-u_{\lambda}$  variations with time, but in a model-dependent way.

#### 3.3 Numerical models

Radiative transfer models are capable of modeling more complex binary phenomena than those allowed by the assumptions of BME (e.g., Kurosawa et al, 2002; Hoffman et al, 2003). Leveraging these models is essential for any deep investigation of specific colliding wind systems. Polarization of spectral lines is especially suited to numerical modeling because of how difficult the problem is in asymmetric geometries.

Numerical models can also be used as initial probes much like BME. Because electron scattering is the primary polarigenic mechanism in hot star winds, the effects of line and continuum polarization can be decoupled by considering their emission and scattering regions. A toy model of the well-studied V444 Cygni has been constructed for this purpose (Fullard, 2020). It is based on the Kurosawa et al (2002) E model of the system including a WR star with an appropriate wind density profile from the Potsdam Wolf-Rayet (PoWR) models<sup>3</sup>. A simple spherical cap cutout represents the O star wind (assumed to be of negligible relative density) at the wind collision point, rotated to mimic the effect of orbital motion. Emission occurs from the WR and O star photospheres (where the WR star photosphere is defined from its PoWR model). It reproduces the continuum behaviour of the system as shown in Figure 10.

To represent line polarization caused by HeII, the emission locations are simply changed to originate from a shell in the WR star wind, and from the edge of the shock region in two clumps. The clumps are located at phase  $\sim 0.12$  and  $\sim 0.75$ , and lie at the edge of the simulation just beyond the O star orbit. Figures 11 and 12 show the resulting polarization curves compared to existing continuum polarization data. Figure 11 shows the complete wind and shock model, which has a

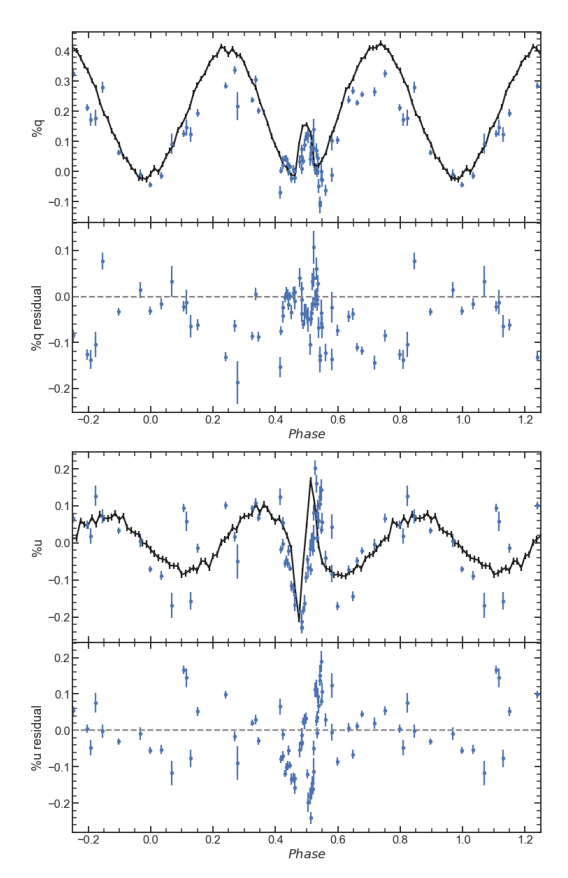


Fig. 10 V444 Cygni polarization (blue points) compared to the Kurosawa et al (2002) E model at an inclination angle of 82.2° (black line), with rotated O star wind cavity as in the emission line model. The *R*-band polarization data are taken from St-Louis et al (1993). Residuals are also presented below each plot. Reproduced with permission.

low near-constant Stokes q and a similar amplitude of variation in Stokes u. Figure 12 shows a model that produces emission only from the two shock regions. This has strong phase-dependent polarization in both Stokes q and u. Neither model produces polarization similar to the continuum signal. Both show the importance of considering line polarization and its capability to diagnose emission regions in colliding winds. It is clear that obtaining polarization observations specifically in spectral lines will provide additional information than that of the continuum polarization.

#### 4 Conclusions

Colliding-wind binaries are important laboratories for the study of radiative wind driving, and massive stars in general, as the detailed structure

<sup>&</sup>lt;sup>3</sup>See the Potsdam PoWR models at the following website: www.astro.physik.uni-potsdam.de/ wrh/PoWR/powr-grid1.php

and geometry of the interaction region between the winds can yield important information about each component's individual wind properties. This interaction is not only due to the bow shock, since the wind from each star can also be influenced by the radiation field from the other star. This phenomenon is best studied with a combination of spectroscopy and polarimetry, and as demonstrated above, the ultraviolet provides an ideal bandpass since the spectral energy distributions of massive stars peak in that region, leading to a wavelength dependence of the polarization.

Several analytical models provide a satisfactory description of the wind collision region, within certain simplifying assumptions detailed in Sect. 3. Our group possesses the ability to leverage these models, as demonstrated for a few illustrative cases.

Using time series of spectropolarimetric observations from Polstar, we will be able to constrain the geometry of the bow shock and therefore the wind properties of a sample of 20 collidingwind binaries spanning a large parameter space. The obtained dataset will significantly improve upon available observations; spectroscopy will be obtained with much higher signal-to-noise ratio and resolution than with IUE and WUPPE, and with greater polarimetric precision than the latter. Achieving a SNR of 100 at spectral resolution down to the wind sound speed, over an orbitally resolved time domain, opens up new and unique wind dynamics diagnostics, as the light from one star scatters in, and is absorbed by, the wind of the other, with orbitally modulated changes in the relevant angles. These produce a more precise mapping between radius and velocity than possible for single stars, allowing tests of the degree to which different wind types and optical depths alter the wind acceleration and structure formation. Information about the bow shock also constrains the relative momentum fluxes in the winds of the two different stars in the binary.

The work described in this paper corresponds to a single science objective included in the *Polstar* proposal, which overlaps in interesting ways with several other objectives described in their own individual papers. We will take advantage of the ways the unique diagnostics supplied by colliding wind binaries informs these other objectives. For example, Gayley et al (2022) discuss how Polstar enables the study of structure and clumping in the winds of the  $\sim 40$  brightest targets, in the context of single stars observed continuously over wind dynamical timescales. Two of those targets,  $\gamma$  Vel and  $\delta$  Ori, are binary systems in the collidingwind target list, so our observations sampled over the system orbit will provide important additional context for the continuous wind dynamics observations. Also, ud-Doula et al (2022) explore the global structural effects of strong magnetization in a subset of OB stars, and a particularly important example is Plaskett's star, which is the only strongly magnetic star observed to also be a rapid rotator. This star is also in our colliding wind target list, and the understanding of its magnetic structure will be complemented by the methods made available by its short-period binary status, as described here.

Closer binaries than the ones examined in this paper can interact and undergo episodes of conservative and nonconservative mass transfer, altering the mass and angular momentum of the binary constituents in ways that are the subject of other Polstar objectives and described in their own papers. ? investigate how UV spectropolarimetry can characterize these mass flows and help determine the fraction of the mass loss by the system, whereas? focus on angular momentum evolution and the pathways for stellar spinup and Keplerian disk creation. UV spectropolarimetry can also provide information regarding the geometry, velocity, and inclination of such disks, as well as the accretion disks of Herbig Ae/Be stars (Wisniewski et al, 2022).

All of these objectives, whose realization will be made possible by Polstar, constrain key evolutionary stages of massive stars and lead to a better understanding of their fates, including the compact objects that they leave behind. Importantly, the analysis of polarization signals from all of these sources will require a detailed understanding of the polarization induced by the intervening interstellar medium; by contributing to improve this knowledge, Polstar will not only enable these topics of stellar physics, but will also yield important insights in the physics of interstellar dust grains (Andersson et al, 2022). Any of these types of systems can, in special cases, provide examples that can be studied over an orbitally modulated range of angles that are either completely sampled, or at least change considerably, over the timeframe of the *Polstar* mission. This paper,

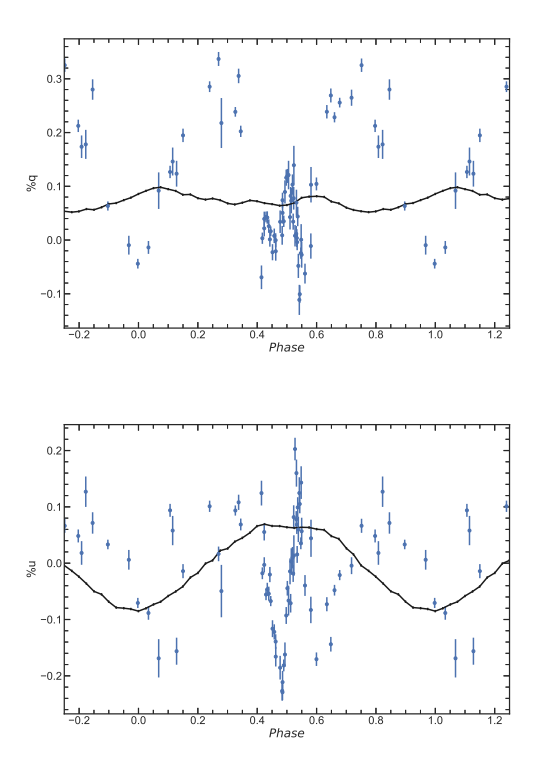


Fig. 11 V444 Cygni polarization (blue points) compared to a wind + shock emission line region model at an inclination angle of 82.2° (black line). The R-band polarization data are taken from St-Louis et al (1993). The comparison between the expected signal in a HeII line from a wind and CWI and the observations in continuum light clearly shows that the signatures are completely different but are both of similar amplitude (in this case only in u). Reproduced with permission.

therefore, is focused on the complementary spectropolarimetric diagnostics available in 20 such cases.

### **Affiliations**

<sup>1</sup>Département de physique, Université de Montréal, Complexe des Sciences, 1375 Avenue Thérèse-Lavoie-Roux, Montréal (Qc), H2V 0B3, Canada

<sup>2</sup>Department of Physics and Astronomy, University of Iowa, Iowa City, IA, 52242

<sup>3</sup>Department of Physics and Astronomy & Pittsburgh Particle Physics, Astrophysics and Cosmology Center (PITT PACC)

<sup>4</sup>Department of Physics & Astronomy, East Tennessee State University, Johnson City, TN 37614, USA

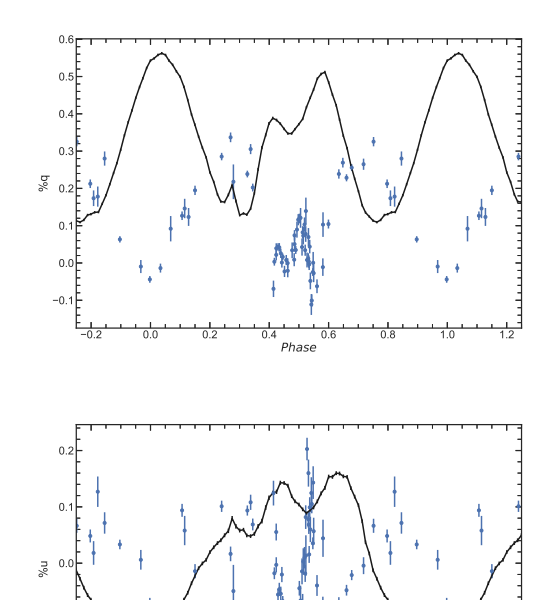


Fig. 12 V444 Cygni polarization (blue points) compared to a shock emission line region model at an inclination angle of 82.2° (black line). The *R*-band polarization data are taken from St-Louis et al (1993). The comparison between the expected signal in a HeII line from a CWI and the observations in continuum light clearly shows that the signatures are completely different but are both of similar amplitude. Reproduced with permission.

<sup>5</sup>Department of Physics and Astronomy, Western University, London, ON N6A 3K7, Canada

<sup>6</sup>Department of Physics and Astronomy, Howard University, Washington, DC 20059, USA

<sup>7</sup>Center for Research and Exploration in Space Science and Technology, and X-ray Astrophysics Laboratory, NASA/GSFC, Greenbelt, MD 20771, USA

<sup>8</sup>Department of Physics and Astronomy, Embry-Riddle Aeronautical University, 3700 Willow Creek Rd, Prescott, AZ, 86301, USA

<sup>9</sup>Armagh Observatory and Planetarium, College Hill, BT61 9DG Armagh, Northern Ireland, UK

<sup>10</sup>Department of Physics & Astronomy, University of Southern California, Los Angeles, CA 90089, USA

<sup>11</sup>Department of Physics & Astronomy, University of Denver, 2112 E. Wesley Ave., Denver, CO 80208, USA

<sup>12</sup>GAPHE, Université de Liège, Allée du 6 Août 19c (B5C), B-4000 Sart Tilman, Liège, Belgium

<sup>13</sup>Department of Physics & Astronomy, University of Auckland, 38 Princes Street, 1010, Auckland, New Zealand

<sup>14</sup>Anton Pannekoek Institute for Astronomy and Astrophysics, University of Amsterdam, 1090 GE Amsterdam, The Netherlands

<sup>15</sup>Department of Physics & Astronomy, Michigan State University,567 Wilson Rd., East Lansing, MI 48824, MI, USA

<sup>16</sup>Physics Department, United States Naval Academy, 572C Holloway Rd, Annapolis, MD 21402, USA

 $^{17}\mathrm{NASA}$  GSFC, Greenbelt , MD 20771, USA

### References

- Andersson, B-G, Clayton GC, et al (2022) Ultraviolet Spectropolarimetry with Polstar: Interstellar Medium Science. Ap&SS 9999:**Topical Collection**
- Auer LH, Koenigsberger G (1994a) Line Profile Variations from Atmospheric Eclipses: Constraints on the Wind Structure in Wolf-Rayet Stars. ApJ436:859. https://doi.org/10.1086/174963
- Auer LH, Koenigsberger G (1994b) Line Profile Variations from Atmospheric Eclipses: Constraints on the Wind Structure in Wolf-Rayet Stars. ApJ436:859. https://doi.org/10. 1086/174963
- Auer LH, van Blerkom D (1972) Electron Scattering in Spherically Expanding Envelopes. ApJ178:175–181. https://doi.org/10.1086/151777
- Bernat AP, Lambert DL (1978) Electron scattering in the expanding atmosphere of P Cygni. PASP90:520–525. https://doi.org/10.1086/130376
- Björklund R, Sundqvist JO, Puls J, et al (2021) New predictions for radiation-driven,

- steady-state mass-loss and wind-momentum hot, massive stars. II. of O-type stars inthe Galaxy and the Magellanic Clouds. A&A648:A36. https://doi.org/10.1051/0004-6361/202038384, https://arxiv.org/abs/arXiv:2008.06066 [astro-ph.SR]
- JC, Hillier Lanz Bouret DJ, T, et al Properties Galactic early-type (2012)of O-supergiants. combined **FUV-UV** analysis. and optical A&A544:A67. https://doi.org/10.1051/0004-6361/201118594, https://arxiv.org/abs/arXiv:1205.3075 [astro-ph.SR]
- Brown DN, Shore SN (1986) Doppler Tomography of the Stellar Wind of the Wolf-Rayet Binary Star V444-CYGNI. In: Rolfe EJ, Wilson R (eds) New Insights in Astrophysics. Eight Years of UV Astronomy with IUE, p 353
- Brown JC, McLean IS, Emslie AG (1978) Polarisation by Thomson scattering in optically thin stellar envelopes. II Binary and multiple star envelopes and the determination of binary inclinations. Astronomy and Astrophysics 68:415–427. URL http://adsabs.harvard.edu/abs/1978A%26A....68..415B
- Brown JC, Aspin C, Simmons JFL, et al (1982) The effect of orbital eccentricity on polarimetric binary diagnostics. Monthly Notices of the Royal Astronomical Society 198:787. https://doi.org/10.1093/mnras/198.3.787, URL https://ui.adsabs.harvard.edu/#abs/1982MNRAS.198..787B/abstract
- Callingham JR, Crowther PA, Williams PM, et al (2020) Two Wolf-Rayet stars at the heart of colliding-wind binary Apep. Monthly Notices of the Royal Astronomical Society 495:3323–3331. https://doi.org/10.1093/mnras/staa1244, URL http://adsabs.harvard.edu/abs/2020MNRAS.495.3323C
- BrottCantiello M, Langer N, I. al (2009)Sub-surface convection zones in hot massive stars and their observable consequences. A&A499:279-290. https://doi.org/10.1051/0004-6361/200911643, https://arxiv.org/abs/arXiv:0903.2049

[astro-ph.SR]

- Cantó J, Raga AC, Wilkin FP (1996) Exact, Algebraic Solutions of the Thin-Shell Two-Wind Interaction Problem. The Astrophysical Journal 469:729. https://doi.org/10.1086/ 177820, URL https://ui.adsabs.harvard.edu/ abs/1996ApJ...469..729C
- Cardelli JA, Clayton GC, Mathis JS (1989) The Relationship between Infrared, Optical, and Ultraviolet Extinction. ApJ345:245. https:// doi.org/10.1086/167900
- Cherepashchuk AM, Eaton JA, Khaliullin KF (1984) Ultraviolet photometry from the Orbiting Astronomical Observatory XXXIX. The structure of the eclipsing Wolf-Rayet binary V444 Cygni as derived from light curves between 2460 A and 3.5 microns. ApJ281:774–788. https://doi.org/10.1086/162156
- Clayton GC, Mathis JS (1988) On the Relationship between Optical Polarization and Extinction. ApJ327:911. https://doi.org/10.1086/166249
- SPCranmer SR.Owocki (1996)Hydrodvnamical Simulations of Corotating Interaction Regions and Discrete Absorption Components in Rotating O-Star Winds. ApJ462:469. https://doi.org/10.1086/177166, https://arxiv.org/abs/arXiv:astro-ph/9508004 [astro-ph]
- Crowther PA, Dessart L, Hillier DJ, et al (2002) Stellar and wind properties of LMC WC4 stars. A metallicity dependence for Wolf-Rayet mass-loss rates. A&A392:653–669. https://doi.org/10.1051/0004-6361:20020941, https://arxiv.org/abs/arXiv:astro-ph/0206233
- Davies B, Oudmaijer RD, Vink JS (2005) Asphericity and clumpiness in the winds of Luminous Blue Variables. A&A439:1107–1125. https://doi.org/10.1051/0004-6361:20052781, https://arxiv.org/abs/arXiv:astro-ph/0505344
- Dessart L, Hillier DJ, Leonard DC (2021)
  Polarization signatures of a high-velocity
  scatterer in nebular-phase spectra of
  Type II supernovae. A&A651:A10.

- https://doi.org/10.1051/0004-6361/202140409, https://arxiv.org/abs/arXiv:2105.01162 [astro-ph.HE]
- Eaton JA, Cherepashchuk AM, Khaliullin KF (1985) Stratification of the Extended Atmosphere of the Wolf-Rayet Component of V444 Cygni. ApJ297:266. https://doi.org/10.1086/163524
- Eversberg T, Lepine S, Moffat AFJ (1998) Outmoving Clumps in the Wind of the Hot O Supergiant zeta Puppis. ApJ494:799–805. https://doi.org/10.1086/305218
- Fox GK (1994) Stellar occultation of polarized light from circumstellar electrons. 4: Detached binary systems. The Astrophysical Journal 432:262–273. https://doi.org/10.1086/174567, URL http://adsabs.harvard.edu/abs/1994ApJ...432..262F
- Fox GK, Hines DC (1998) The polarimetric nature of HD 108. MNRAS295:423–427. https://doi.org/10.1046/j.1365-8711.1998.01296.x
- Fullard AG (2020) A spectropolarimetric study of Wolf-Rayet binary stars. PhD thesis, University of Denver, United States
- Fullard AG, St-Louis N, Moffat AFJ, et al Multiwavelength Search for (2020)Α Intrinsic Linear Polarization in Wolf-Ravet Winds. AJ159(5):214. https: //doi.org/10.3847/1538-3881/ab8293, https://arxiv.org/abs/arXiv:1912.12249 [astro-ph.SR]
- Fullerton AW, Massa DL, Prinja RK (2006) The Discordance of Mass-Loss Estimates for Galactic O-Type Stars. ApJ637:1025– 1039. https://doi.org/10.1086/498560, https://arxiv.org/abs/arXiv:astro-ph/0510252
- Gayley KG (2009)Asymptotic Open-Angles for Colliding-Wind Bow ing Shocks: The Characteristic-Angle ApJ703(1):89-95. Approximation. https: //doi.org/10.1088/0004-637X/703/1/89. https://arxiv.org/abs/arXiv:0905.1395 [astro-ph.SR]

- Gayley KG, Vink JS, ud Doula A, et al (2022) Understanding Structure in Line-Driven Stellar Winds Using Ultraviolet Spectropolarimetry in the Time Domain. Ap&SS 9999:**Topical** Collection
- Georgiev LN, Koenigsberger G (2004) Line profile variations in WR+O binary systems. I. The code and basic predictions. Astronomy and Astrophysics, v423, p267-279 (2004) 423:267. https://doi.org/10.1051/0004-6361:200400030, URL https://ui.adsabs.harvard.edu/abs/2004A%26A...423..267G/abstract
- Girard T, Willson LA (1987) Winds in collision. III. Modeling the interaction nebulae of eruptivesymbiotics. Astronomy and Astrophysics, Vol 183, p 247-256 (1987) 183:247. URL https://ui.adsabs.harvard.edu/abs/1987A%26A...183..247G/abstract
- Gosset E, Nazé Y, Sana H, et al (2009) Phase-resolved XMM-Newton observations of the massive WR+O binary WR 22. A&A508(2):805–821. https://doi.org/10.1051/ 0004-6361/20077981
- Gräfener G, Hamann WR (2005)Hvdrodynamic model atmospheres for WR stars. Self-consistent modeling WC star wind. A&A432:633–645. https: //doi.org/10.1051/0004-6361:20041732, https://arxiv.org/abs/arXiv:astro-ph/0410697
- Gräfener G, Koesterke L, Hamann WR (2002) Line-blanketed model atmospheres for WR stars. A&A387:244–257. https://doi.org/10.1051/0004-6361:20020269
- Gräfener G, Owocki SP, Vink JS (2012) Stellar envelope inflation near the Eddington limit. Implications for the radii of Wolf-Rayet stars and luminous blue variables. A&A538:A40. https://doi.org/10.1051/0004-6361/201117497, https://arxiv.org/abs/arXiv:1112.1910 [astro-ph.SR]
- Grassitelli L, Chené AN, Sanyal D, et al (2016) Diagnostics of the unstable envelopes of Wolf-Rayet stars. A&A590:A12. https://doi.org/10.1051/0004-6361/201527873, https://arxiv.org/abs/arXiv:1603.08931

- [astro-ph.SR]
- R, Ramachandran V, Shenar T, Hainich (2019)PoWRgrids of non-LTE atmospheres OB-type model for of various metallicities. A&A621:A85. https://doi.org/10.1051/0004-6361/201833787, https://arxiv.org/abs/arXiv:1811.06307 [astro-ph.SR]
- Hamann WR, Koesterke L (1998) Spectrum formation in clumped stellar winds: consequences for the analyses of Wolf-Rayet spectra. A&A335:1003–1008
- Harries TJ, Hillier DJ, Howarth ID (1998) A spectropolarimetric survey of northern hemisphere Wolf-Rayet stars. MNRAS296(4):1072–1088. https://doi.org/10.1046/j.1365-8711.1998. 01508.x
- Harries TJ, Babler BL, Fox GK (2000) The polarized spectrum of the dust producing Wolf-Rayet+O-star binary WR137. A&A361:273–282
- Hillier DJ (1984) The influence of electron scattering on the He II line profiles in HD50896. ApJ280:744–748. https://doi.org/10.1086/162047
- Hillier DJ (1991) The effects of electron scattering and wind clumping for early emission line stars. A&A247:455–468
- Hillier DJ, Miller DL (1999) Constraints on the Evolution of Massive Stars through Spectral Analysis. I. The WC5 Star HD 165763. ApJ519:354–371. https://doi.org/10. 1086/307339
- Hillier DJ, Lanz T, Heap SR, et al (2003) A
  Tale of Two Stars: The Extreme O7 Iaf+
  Supergiant AV 83 and the OC7.5 III((f)) star
  AV 69. ApJ588:1039–1063. https://doi.org/10.
  1086/374329
- Hoffman JL (2007) Polarized Line Profiles as Diagnostics of Circumstellar Geometry in Type IIn Supernovae. In: Revista Mexicana de Astronomia y Astrofisica Conference Series, pp 57–63, astro-ph/0612244

- Hoffman JL, Nordsieck KH, Fox GK (1998) Spectropolarimetric Evidence for a Bipolar Flow in beta Lyrae. AJ115(4):1576–1591. https://doi.org/10.1086/300274
- Hoffman JL, Whitney BA, Nordsieck KH (2003) The Effect of Multiple Scattering on the Polarization from Binary Star Envelopes. I. Self- and Externally Illuminated Disks. ApJ598(1):572–587. https://doi.org/10.1086/378770, https://arxiv.org/abs/arXiv:astro-ph/0307261 [astro-ph]
- Howarth ID, Prinja RK (1989) The stellar winds of 203 Galactic O stars A quantitative ultraviolet survey. ApJS69:527–592. https://doi.org/10.1086/191321
- Huk LN (2017) Time-dependent spectropolarimetric modeling of interacting core collapse supernovae. PhD thesis, University of Denver, United States
- Ignace R (2000a) Polarization from Be Disks with 1-Armed Density Waves. In: Smith MA, Henrichs HF, Fabregat J (eds) IAU Colloq. 175: The Be Phenomenon in Early-Type Stars, p 452
- Ignace R (2000b) Resonance line scattering polarization in optically thin planar equatorial disks. A&A363:1106–1114
- Ignace R, Al-Malki MB, Simmons JFL, et al (2009) Scattering polarization due to light source anisotropy. II. Envelope of arbitrary shape. A&A496(2):503–511. https://doi.org/10.1051/0004-6361:200811214
- Ignace R, Fullard A, Shrestha M, et al (2022) Modeling the Optical to Ultraviolet Polarimetric Variability from Thomson Scattering in Colliding Wind Binaries. arXiv e-prints arXiv:2205.07612. https://arxiv.org/abs/arXiv:2205.07612 [astro-ph.SR]
- Ishii M, Ueno M, Kato M (1999) Core-Halo Structure of a Chemically Homogeneous Massive Star and Bending of the Zero-Age Main Sequence. PASJ51:417–424. https://doi.org/10.1093/pasj/51.4.417, https://arxiv.org/abs/astro-ph/9907154

- Jeffery DJ (1989) The Soboloev-P Method: A Generalization of the Sobolev Method for the Treatment of the Polarization State of Radiation and the Polarizing Effect of Resonance Line Scattering. ApJS71:951. https://doi.org/10.1086/191404
- Jones CE, Labadie-Bartz J, Cotton DV, et al (2022) Ultraviolet Spectropolarimetry: on the origin of rapidly rotating B stars. Ap&SS 9999:**Topical Collection**
- Kallrath J (1991) Dynamics of colliding binary stellar winds pressure equilibrium models. Monthly Notices of the Royal Astronomical Society 248:653. https://doi.org/10.1093/mnras/248.4.653, URL https://ui.adsabs.harvard.edu/abs/1991MNRAS.248..653K
- Kaper L, Henrichs HF, Nichols JS, et al (1996) Long- and short-term variability in O-star winds. I. Time series of UV spectra for 10 bright O stars. A&AS116:257–287
- Kennedy M, Dougherty SM, Fink A, et al (2010) Modeling the Radio Emission from Cyg OB2 No. 5: A Quadruple System? ApJ709(2):632–643. https://doi.org/10.1088/0004-637X/709/2/632, https://arxiv.org/abs/arXiv:0911.5674 [astro-ph.SR]
- Koenigsberger G (1990) The Fe V/Fe VI ionization structure in WNE Wolf-Rayet winds. A&A235:282
- Koenigsberger G, Auer LH (1985) IUE observations of phase-dependent variations in WN+O systems. ApJ297:255–265. https://doi.org/10.1086/163523
- Kurosawa R, Hillier DJ, Pittard JM (2002) Mass-loss rate determination for the massive binary V444 Cygni using 3-D Monte-Carlo simulations of line and polarization variability. Astronomy and Astrophysics 388:957–977. https://doi.org/10.1051/0004-6361:20020443, URL http://adsabs.harvard.edu/abs/2002A% 26A...388..957K
- Lamberts A, Fromang S, Dubus G (2011) Highresolution numerical simulations of unstable colliding stellar winds. Monthly Notices of the

- Royal Astronomical Society 418:2618–2629.  $\label{eq:https:/doi.org/10.1111/j.1365-2966.2011.} \\ 19653.x, URL https://ui.adsabs.harvard.edu/abs/2011MNRAS.418.2618L$
- Leonard DC, Dessart L, Hillier DJ, et al (2021) A High-Velocity Scatterer Revealed in the Thinning Ejecta of a Type II Supernova. arXiv e-prints arXiv:2110.10875. https://arxiv.org/abs/arXiv:2110.10875 [astro-ph.HE]
- Lépine S, Moffat AFJ (1999) Wind Inhomogeneities in Wolf-Ravet Stars. II. Investigation **Emission-Line** Proof Variations. ApJ514:909-931. file https: //doi.org/10.1086/306958
- Lomax JR, Nazé Y, Hoffman JL, et al (2015) V444 Cygni X-ray and polarimetric variability: Radiative and Coriolis forces shape the wind collision region. A&A573:A43. https://doi.org/10.1051/0004-6361/201424468, https://arxiv.org/abs/arXiv:1410.6117 [astro-ph.SR]
- Lucy LB (2007) Mass fluxes for O stars. A&A468:649–655. https://doi.org/10.1051/0004-6361:20077298, https://arxiv.org/abs/arXiv:astro-ph/0703650
- Luehrs S (1997) A Colliding-Wind Model for the Wolf-Rayet System HD 152270. PASP109:504– 513. https://doi.org/10.1086/133907
- MacLeod Μ. Loeb Α (2020)Hydrody-Winds Twin-star namic fromBinaries. The Astrophysical Journal 902:85. //doi.org/10.3847/1538-4357/abb313, URL https://ui.adsabs.harvard.edu/abs/2020ApJ... 902...85M
- Maeder A (1981) Evolution and nucleosynthesis in massive stars with mass loss The yields in helium and heavy elements and constraints on the past star formation rate. A&A101:385–396
- Martin PG, Clayton GC, Wolff MJ (1999) Ultraviolet Interstellar Linear Polarization. V. Analysis of the Final Data Set. ApJ510(2):905–914. https://doi.org/10.1086/306613

- Massa D, Fullerton AW, Sonneborn G, et al (2003) Constraints on the Ionization Balance of Hot-Star Winds from FUSE Observations of O Stars in the Large Magellanic Cloud. ApJ586:996– 1018. https://doi.org/10.1086/367786, https://arxiv.org/abs/arXiv:astro-ph/0211518
- G, Chomienne V, S. Meynet Ekström et al (2015)Impact of mass-loss on evolution and pre-supernova the propof red supergiants. A&A575:A60. https://doi.org/10.1051/0004-6361/201424671, https://arxiv.org/abs/arXiv:1410.8721 [astro-ph.SR]
- Mossoux Ε. Rauw G (2021)LIFELINE: The program the simulation for the X-ray line profiles in massive colliding wind binaries. A&A646:A89. https://doi.org/10.1051/0004-6361/202039437, https://arxiv.org/abs/arXiv:2011.14866 [astro-ph.IM]
- Mullan DJ (1986) Displaced narrow absorption components in the spectra of mass-losing OB stars: indications of corotating interaction regions? A&A165:157–162
- Nazé Y, Koenigsberger G, Pittard JM, et al (2018) A Changing Wind Collision. ApJ853(2):164. https://doi.org/10.3847/1538-4357/aaa29c, https://arxiv.org/abs/arXiv:1712.05625 [astro-ph.SR]
- Nugis T, Lamers HJGLM (2000) Mass-loss rates of Wolf-Rayet stars as a function of stellar parameters. A&A360:227-244
- Oskinova LM, Hamann WR, Feldmeier A (2007) Neglecting the porosity of hotstar winds can lead to underestimating mass-loss rates. A&A476(3):1331–1340. https://doi.org/10.1051/0004-6361:20066377, https://arxiv.org/abs/arXiv:0704.2390 [astro-ph]
- Owocki SP (2008) Dynamical simulation of the "velocity-porosity" reduction in observed strength of stellar wind lines. In: Hamann WR, Feldmeier A, Oskinova LM (eds) Clumping in Hot-Star Winds, p 121

- Parkin ER, Pittard JM, Corcoran MF, et al (2009) 3D modelling of the colliding winds in  $\eta$  Carinae evidence for radiative inhibition. MNRAS394(4):1758–1774. https://doi.org/10.1111/j.1365-2966.2009.14475.x, https://arxiv.org/abs/arXiv:0901.0862 [astro-ph.HE]
- Paxton B, Bildsten L, Dotter A, et al (2011) Modules for Experiments in Stellar Astrophysics (MESA). ApJS192(1):3. https://doi.org/10.1088/0067-0049/192/1/3, https://arxiv.org/abs/arXiv:1009.1622 [astro-ph.SR]
- Peters GJ, Gayley KG, Ignace R, et al (2022) Ultraviolet Spectropolarimetry: Conservative and Nonconservative Mass Transfer in OB Interacting Binaries. Ap&SS 9999:**Topical** Collection
- Petrovic J, Pols O, Langer N (2006) Are luminous and metal-rich Wolf-Rayet stars inflated? A&A450:219-225. https://doi.org/10. 1051/0004-6361:20035837
- Pittard JM (2009) 3D models of radiatively driven colliding winds in massive O+O star binaries I. Hydrodynamics. MNRAS396(3):1743–1763. https://doi.org/10.1111/j.1365-2966.2009.14857.x, https://arxiv.org/abs/arXiv:0904.0164 [astro-ph.SR]
- Rauw G, Nazé Y, Carrier F, et al (2001) The strange case of the massive binary HD 149404. A&A368:212-224. https://doi.org/10.1051/0004-6361:20000527
- Rauw G, Vreux JM, Stevens IR, et al (2002) Phase-resolved X-ray and optical spectroscopy of the massive binary HD 93403. A&A388:552– 562. https://doi.org/10.1051/0004-6361: 20020523
- Rauw G. Mossoux Ε, Nazé Y (2016)Fe XXV line profiles in colliding wind binaries. New Astron.43:70–79. https: //doi.org/10.1016/j.newast.2015.08.002, https://arxiv.org/abs/arXiv:1508.04965 [astro-ph.SR]

- Russell CMP, Wang QD, Cuadra J (2017) Modelling the thermal X-ray emission around the Galactic Centre from colliding Wolf-Rayet winds. MNRAS464(4):4958–4965. https://doi.org/10.1093/mnras/stw2584, https://arxiv.org/abs/arXiv:1607.01562 [astro-ph.HE]
- Sana H, Rauw G, Gosset E (2001) HD 152248: Evidence for a colliding wind interaction. A&A370:121-135. https://doi.org/10.1051/0004-6361:20010221
- Sana H, Nazé Y, O'Donnell B, et al (2008) The massive binary HD 152218 revisited: A new colliding wind system in NGC 6231. New Astron.13(4):202–215. https://doi.org/10.1016/j.newast.2007.07.008, https://arxiv.org/abs/arXiv:0801.3753 [astro-ph]
- Sana H, de Mink SE, de Koter A, et al (2012) Binary Interaction Dominates the Evolution of Massive Stars. Science 337(6093):444. https://doi.org/10.1126/science.1223344, URL https://ui.adsabs.harvard.edu/#abs/2012Sci... 337..444S/abstract
- Sander A, Hamann WR, Todt H (2012) The Galactic WC stars. Stellar parameters from spectral analyses indicate a new evolutionary sequence. A&A540:A144. https://doi.org/10.1051/0004-6361/201117830, https://arxiv.org/abs/arXiv:1201.6354 [astro-ph.SR]
- Sander A, Shenar T, Hainich R, et (2015)On the consistent treatment quasi-hydrostatic layers of the hot atmospheres. A&A577:A13. https: //doi.org/10.1051/0004-6361/201425356, https://arxiv.org/abs/arXiv:1503.01338 [astro-ph.SR]
- Sander AAC, Vink JS, Hamann WR (2020) Driving classical Wolf-Rayet winds: a Γ- and Z-dependent mass-loss. MNRAS491(3):4406– 4425. https://doi.org/10.1093/mnras/stz3064, https://arxiv.org/abs/arXiv:1910.12886 [astro-ph.SR]

- Schulte-Ladbeck RE, Nordsieck KH, Nook MA, et al (1990) A Rotating, Expanding Disk in the Wolf-Rayet Star EZ Canis Majoris? ApJ365:L19. https://doi.org/10.1086/185878
- Schulte-Ladbeck RE, Nordsieck KH, Code AD, et al (1992) The First Linear Polarization Spectra of Wolf-Rayet Stars in the Ultraviolet: EZ Canis Majoris and theta MUSCAE. ApJ391:L37. https://doi.org/10.1086/186393
- Scowen PA, Gayley KG, Ignace R, et al (2022) The Polstar High Resolution Spectropolarimetry MIDEX Mission. Ap&SS 9999:**Topical** Collection
- Shenar T, Oskinova L, Hamann WR, et al (2015) A Coordinated X-Ray and Optical Campaign of the Nearest Massive Eclipsing Binary,  $\delta$  Orionis Aa. IV. A Multiwavelength, Non-LTE Spectroscopic Analysis. ApJ809(2):135. https://doi.org/10.1088/0004-637X/809/2/135, https://arxiv.org/abs/arXiv:1503.03476 [astro-ph.SR]
- Shrestha M, Neilson HR, Hoffman JL, et al (2018) Polarization simulations of stellar wind bow-shock nebulae I. The case of electron scattering. MNRAS477(1):1365–1382. https://doi.org/10.1093/mnras/sty724, https://arxiv.org/abs/arXiv:1712.04958 [astro-ph.SR]
- Shrestha M, Neilson HR, Hoffman JL, et al (2021) Polarization simulations of stellar wind bow shock nebulae II. The case of dust scattering. MNRAS500(4):4319–4337. https://doi.org/10.1093/mnras/staa3508, https://arxiv.org/abs/arXiv:2011.04314 [astro-ph.SR]
- Sobolev VV (1960) Moving envelopes of stars. Harvard Univ. Press, Cambridge
- St-Louis N, Moffat AFJ, Lapointe L, et al (1993) Polarization Eclipse Model of the Wolf-Rayet Binary V444 Cygni with Constraints on the Stellar Radii and an Estimate of the Wolf-Rayet Mass-Loss Rate. The Astrophysical Journal 410:342. https://doi.org/10.1086/172751, URL https://ui.adsabs.harvard.edu/abs/1993ApJ...410..342S/abstract

- St-Louis N, Willis AJ, Stevens IR (1993) Ultraviolet Observations of Selective Wind Eclipses in gamma Velorum and Evidence for Colliding Winds. ApJ415:298. https://doi.org/10.1086/173165
- Stevens IR, Blondin JM, Pollock AMT (1992) Colliding Winds from Early-Type Stars in Binary Systems. The Astrophysical Journal 386:265. https://doi.org/10.1086/171013, URL https://ui.adsabs.harvard.edu/?#abs/ 1992ApJ...386..265S/abstract
- Tuthill PG, Monnier JD, Danchi WC (1999)
  A dusty pinwheel nebula around the massive star WR104. Nature398(6727):487–489. https://doi.org/10.1038/19033, https://arxiv.org/abs/arXiv:astro-ph/9904092 [astro-ph]
- ud-Doula A, Cheung MCM, David-Uraz A, et al (2022) Ultraviolet Spectropolarimetric Diagnostics of Hot Star Magnetospheres. Ap&SS 9999:**Topical Collection**
- Villar-Sbaffi A, St-Louis N, Moffat AFJ, et al (2005) First Ever Polarimetric Detection of a Wind-Wind Interaction Region and a Misaligned Flattening of the Wind in the Wolf-Rayet Binary CQ Cephei. ApJ623(2):1092–1104. https://doi.org/10.1086/428830
- Vink JS, Sander AAC (2021) Metallicity-dependent wind parameter predictions for OB stars. MNRAS504(2):2051–2061. https://doi.org/10.1093/mnras/stab902, https://arxiv.org/abs/arXiv:2103.12736 [astro-ph.SR]
- Vink JS, de Koter A, Lamers HJGLM (2001) Mass-loss predictions for O and B stars as a function of metallicity. A&A369:574–588. https://doi.org/10.1051/0004-6361:20010127, https://arxiv.org/abs/arXiv:astro-ph/0101509
- Williams PM (2019) Variable dust emission by WC type Wolf-Rayet stars observed in the NEOWISE-R survey. MNRAS488(1):1282– 1300. https://doi.org/10.1093/mnras/stz1784, https://arxiv.org/abs/arXiv:1906.11595 [astroph.SR]

Williams PM, van der Hucht KA, Pollock AMT, et al (1990) Multi-frequency variations of the Wolf-rayet system HD 193793 - I. Infrared, X-ray and radio observations. MNRAS243:662–684

Williams PM, Rauw G, van der Hucht KA (2009) Dust formation by the colliding wind WC5+O9 binary WR19 at periastron passage. MNRAS395(4):2221-2225. https://doi.org/10.1111/j.1365-2966.2009.14681.x, https://arxiv.org/abs/arXiv:0902.4105 [astro-ph.SR]

Wisniewski JP, Berdyugin A, Berdyugina S, et al (2022) UV Spectropolarimetry with Polstar: Protoplanetary Disks. Ap&SS 9999:**Topical** Collection

# Ackowledgments & Declarations

Acknowledgments. RI acknowledges funding support from a grant by the National Science Foundation (NSF), AST-2009412. JLH acknowledges support from NSF under award AST-1816944 and from the University of Denver via a 2021 PROF award. Scowen acknowledges his financial support by the NASA Goddard Space Flight Center to formulate the mission proposal for Polstar. Y.N. acknowledges support from the Fonds National de la Recherche Scientifique (Belgium), the European Space Agency (ESA) and the Belgian Federal Science Policy Office (BELSPO) in the framework of the PRODEX Programme (contracts linked to XMM-Newton and Gaia). NSL and CEJ wish to thank the National Sciences and Engineering Council of Canada (NSERC) for financial support. A.D.-U. is supported by NASA under award number 80GSFC21M0002. GJP gratefully acknowledges support from NASA grant 80NSSC18K0919 and STScI grants HST-GO-15659.002 and HST-GO-15869.001.

#### **Declarations**

#### **Funding**

The Polstar satellite is presently being proposed as a Midex mission to NASA and is currently under evaluation.

#### **Author Contribution**

All authors have contributed ideas to motivate the work presented in this paper. Some have provided specific modelling, others proposed data analysis techniques. All contributed to the writing of the text to varying extents.

### **Competing Interests**

To our knowledge, there are no competing interests.

#### Data Availability

The team will make the data obtained within the context of this mission available to the astronomical community.